Synergies between *Planck* & future CMB missions and radio sky studies

Carlo Burigana
@ INAF/IASF Bologna

thanks to the *Planck* & PRISM Collaborations & Italian SKA Working Group for related topics

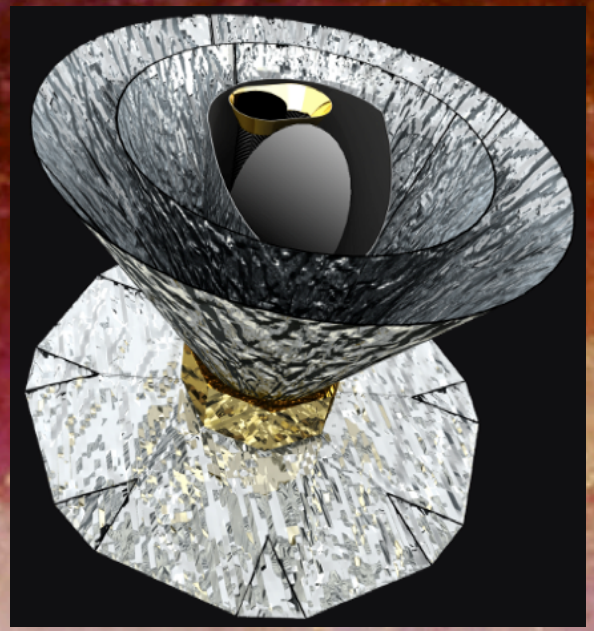

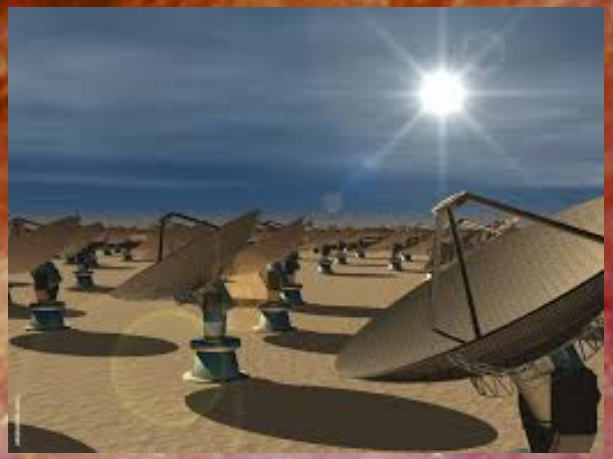

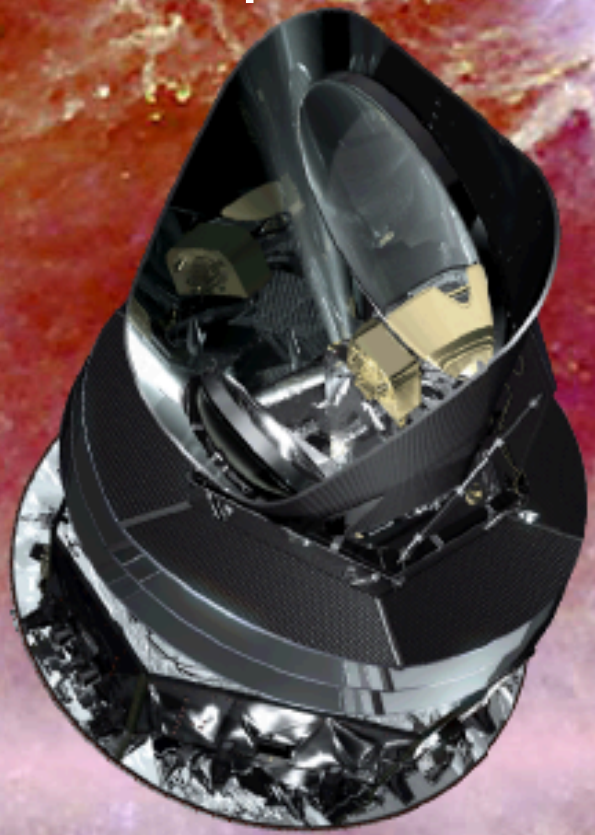

43rd Young European Radio Astronomer Conference
(YERAC)
30 September – 3 October 2013
Bielefeld University, Germany

OUTLINE

- *Planck* "in brief" … as long as possible ☺
  - Mission & products
  - Main cosmological results
- Future CMB missions (crossing fingers ☺)
- SKA science … from the point of view of synergies with CMB (see Ben Stappers's talk for SKA description)
  - SZ from clusters
  - SZ @ galaxy scales
  - Implications for CMB spectrum studies
  - Free-free signals @ various epochs ←→ reionization
  - Cross-correlations CMB←→ RS catalogues
  - Primordial Magnetic Fields
  - Galactic diffuse emission

Some References (on synergies parts)

[1] Sunvaev R.A., Zeldovich Ya.B., 1972, Comm. Astrophys. Space Phys., 4, 173
[2] Rephaeli Y., 1995, ARA&A, 33, 541
[3] Rees M.J., Ostriker J.P., 1977, MNRAS, 179, 541
[4] White S.D.M., Rees M.J., 1978, MNRAS, 183, 341
[5] Ikeuchi S., 1981, PASJ, 33, 211
[6] Platania P., Burigana C., De Zotti G., Lazzaro E., Bersanelli M., 2002, MNRAS, 337, 242
[7] Lapi A., Cavaliere A., De Zotti G., 2003, ApJ, 597, L93
[8] Burigana C., de Zotti G., Feretti L., 2004, New Astronomy Reviews, 48, 1107
[9] Pei Y.,1995, ApJ, 438, 623
[10] Oh S.P., 1999, ApJ, 527, 16
[11] Partridge R.B., Richards E.A., Fomalont E.B., Kllerman K.I., Windhorst R., 1997 ApJ, 483, 38
[12] Ponente P.P., Diego J.M., Sheth R.K., Burigana C., Knollmann S.R., Ascasibar Y., 2011, MNRAS, 410, 2353
[13] Trombetti T., Burigana C., 2013, will appear on MNRAS
[14] Feretti L., et al., Italian SKA White Book, 2013
[15] Tegmark M., 1997, Phys. Rev. D, 55, 5895
[16] Sachs R.K., Wolfe A.M., 1967, ApJ, 147, 73
[17] Crittenden R.G., Turok N., 1996, Physical Review Letters, 76, 575
[18] Raccanelli A., Bonaldi A., Negrello M., et al. 2008,MNRAS, 386, 2161
[19] Schiavon F., Finelli F., Gruppuso A., et al., 2012, MNRAS, 427, 3044
[20] Xia J.Q., Baccigalupi C., Matarrese S., Verde L., Viel M., 2011, JCAP, 08, 033
[21] Ryu D., Schleicher D.R.G., Treumann R.A., Tsagas C.G., Widrow L.M., 2012, Space Sci. Rev., 166, 1
[22] Widrow L.M., Ryu D., Schleicher D.R.G., et al., 2012, Space Sci. Rev., 166, 37
[23] Paoletti D., Finelli F., 2011, Phys. Rev. D, 83, 123533
[24] Caprini C., Finelli F., Paoletti D., Riotto A., 2009, JCAP, 6, 21
[25] Neronov A., Vovk I., 2010, Science, 328, 5974 73
[26] Burigana C., La Porta L., Reich P., Reich W., 2006, AN, 327, 491
[27] Bennett C.L., Larson D., Weiland J.L., et al., 2013, ApJS, submitted, arXiv:1212.5225

The scientific results that we present today are a product of the Planck Collaboration, including individuals from more than 100 scientific institutes in Europe, the USA and Canada

Planck is a project of the European Space Agency, with instruments provided by two scientific Consortia funded by ESA member states (in particular the lead countries: France and Italy) with contributions from NASA (USA), and telescope reflectors provided in a collaboration between ESA and a scientific Consortium led and funded by Denmark.

CMB space mission experiments overview – Planck: 3rd Generation

The oldest light or the first light of the Universe

1965 — Penzias and Wilson

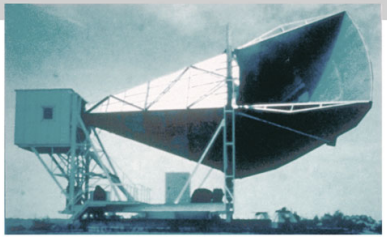

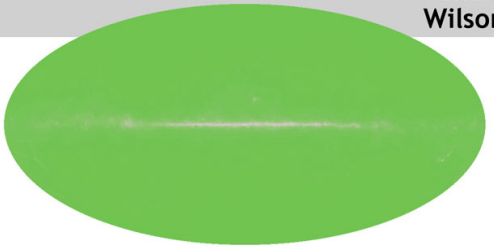

Discovered the remnant afterglow from the **Big Bang**.
→ **2.7 K**

1992 — COBE

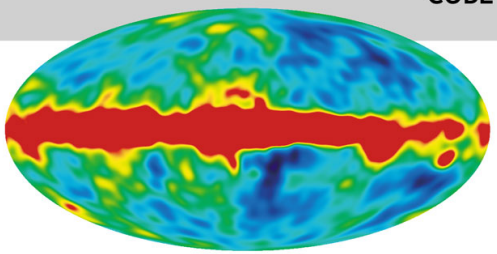

Blackbody radiation, Discovered the patterns (**anisotropy**) in the afterglow.
→ **angular scale ~ 7°** at a level ΔT/T of 10^{-5}

2003 — WMAP

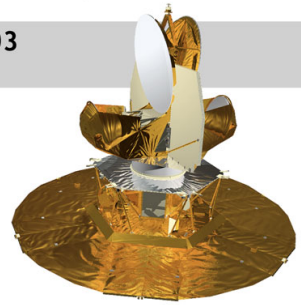

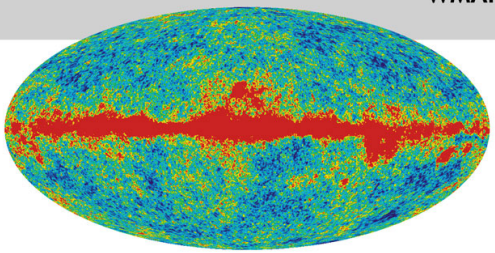

(Wilkinson Microwave Anisotropy Probe):
→ **angular scale ~ 15'**

2009 — *Planck*

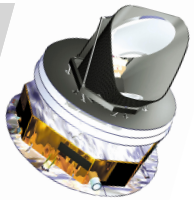

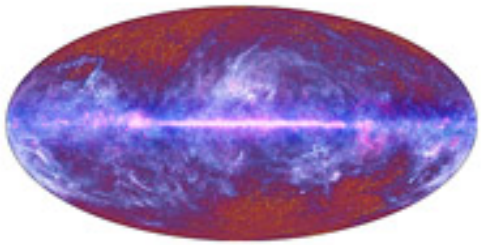

→ **angular scale ~ 5',**
ΔT/T ~ 2×10^{-6}, 30~867 Hz

Planck is composed by two instruments:

- The Low Frequency Instrument (LFI) based on EMT receivers and
- The High Frequency Instrument (HFI) based on bolometers

@ focal plane of a1.5 m Gregorian telescope

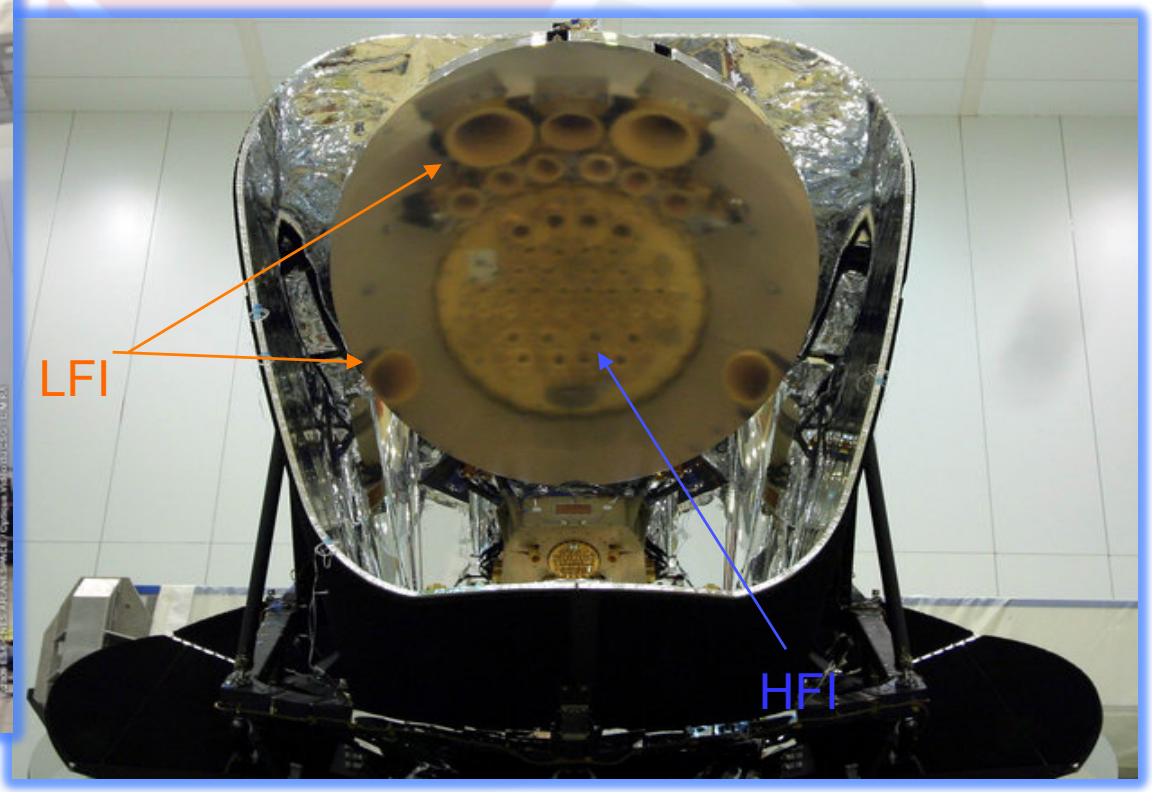

PLANCK HAS BEEN SUCCESSFULLY LAUNCHED ON THE 14 OF MAY 2009, TOGETHER WITH HERSCHEL, ON ARIANE 5 VECTOR

Is acquiring data since the 15 August 2009,

In January 2012 HFI was switched off and since then Planck is in LFI only mode

Survey	Instrument	Beginning	End	Coverage[a]
1	LFI & HFI	12 August 2009 (14:16:51 UT)	2 February 2010 (20:51:04 UT)	93.1 %
2	LFI & HFI	2 February 2010 (20:54:43)	12 August 2010 (19:27:20 UT)	93.1 %
3[b]	LFI & HFI	12 August 2010 (19:30:44)	8 February 2011 (20:55:55 UT)	93.1 %
4	LFI & HFI	8 February 2011 (20:59:10)	29 July 2011 (17:13:32)	86.6 %
5[c]	LFI & HFI	29 July 2011 (18:04:49)	1 February 2012 (05:26:29 UT)	80.1 %
6	LFI	14 January 2012	July 2012	
7	LFI	July 2012	Jan 2013	
8	LFI	Jan 2013	August 2013	

[a] Fraction of the sky covered by all frequencies
[b] End of Nominal period = 28 November 2010 (12:00:53 UT)
[c] End of data acquisition with HFI = 13 January 2012 (14:54:07 UT)

Planck Scanning Strategy

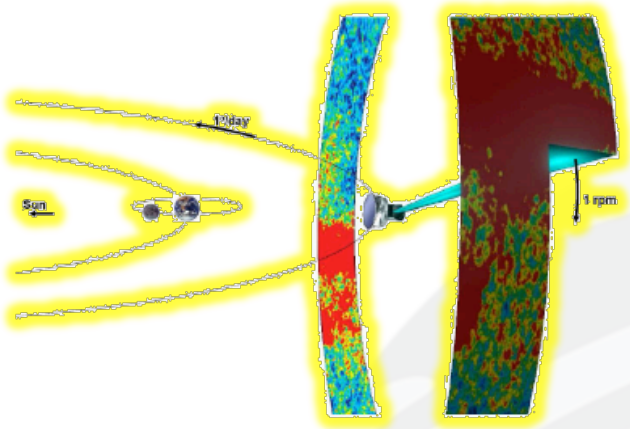

Planck is a survey mission

About 6 months are needed to cover ~95% of the sky.

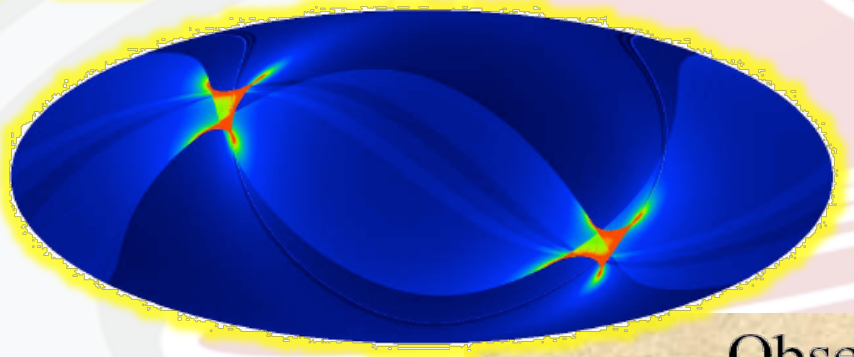

Survey ≥ 5:
cycloid phase shifted by 90 deg.

During LFI only phase (surveys 6-8):
scanning strategy combines standard mode with deep annuli on calibration sources to improve the quality of calibration and systematic effect control.

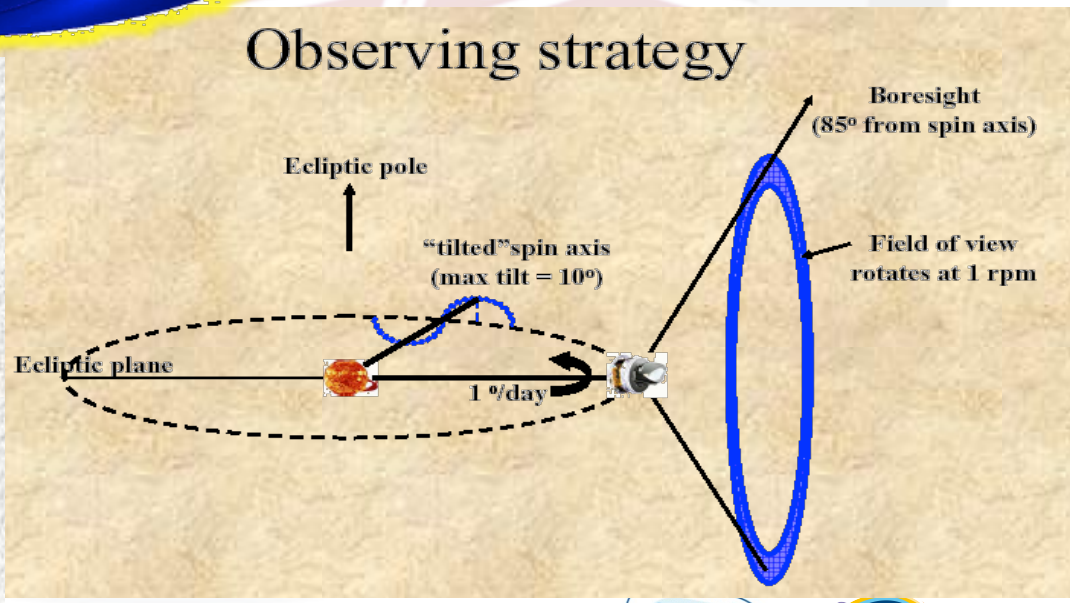

PLANCK IN SUMMARY: 9 FREQUENCIES BETWEEN 30 GHz AND 1 THz

Channel	$N_{detectors}$[a]	ν_{center}[b] [GHz]	Scanning Beam[c] FWHM [arcm]	Scanning Beam[c] Ellipticity	Noise[d] Sensitivity [$\mu K_{RJ}\ s^{1/2}$]	Noise[d] Sensitivity [$\mu K_{CMB}\ s^{1/2}$]
30 GHz	4	28.4	33.16	1.37	145.4	148.5
44 GHz	6	44.1	28.09	1.25	164.8	173.2
70 GHz	12	70.4	13.08	1.27	133.9	151.9
100 GHz	8	100	9.59	1.21	31.52	41.3
143 GHz	11	143	7.18	1.04	10.38	17.4
217 GHz	12	217	4.87	1.22	7.45	23.8
353 GHz	12	353	4.7	1.2	5.52	78.8
545 GHz	3	545	4.73	1.18	2.66	0.0259[d]
857 GHz	4	857	4.51	1.38	1.33	0.0259[d]

FOR TEMPERATURE ANALYSES

PLANCK SENSITIVITY AND ANGULAR RESOLUTION ARE ENOUGH TO BE ESSENTIALLY COSMIC VARIANCE LIMITED … BUT ALSO LIMITED (ONLY) BY THE CAPABILITY TO REMOVE THE CONTAMINATION BY ASTROPHYSICAL SIGNAL

WIDE FREQUENCY RANGE CLEARLY HELPS

HOW TO EXTRACT INFORMATION FROM THE MEASUREMENTS

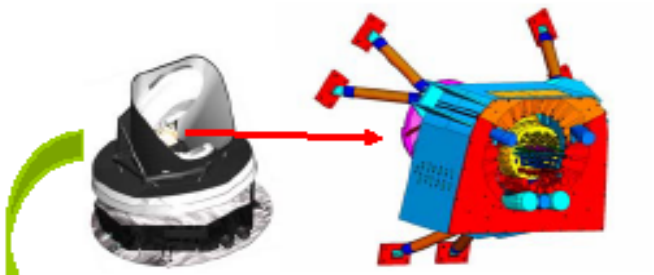

Acquiring and processing
time-ordered information

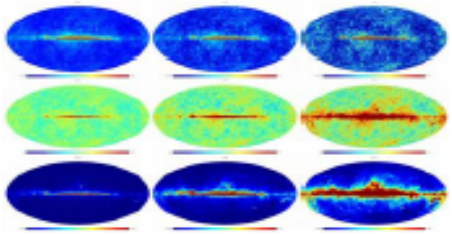

Converting time-ordered data
to maps of the sky emission
at many frequencies

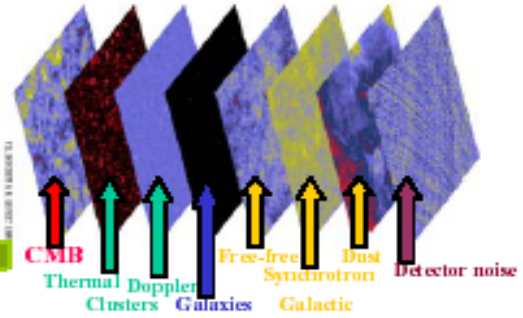

Converting frequency
maps to component maps,
e.g. the Cosmic Microwave Background

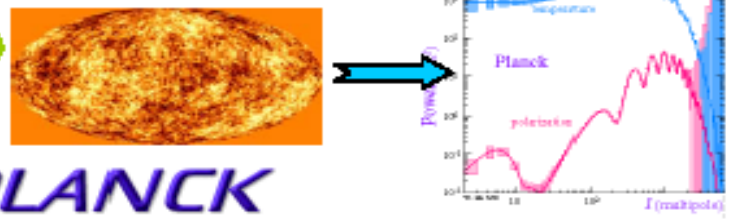

Estimating the CMB
angular power spectrum
and cosmological parameters

PLANCK

esa ASTROPHYSICS

Zodiacal emission

...measured by IRAS (it's the white 'S', not the Galaxy)

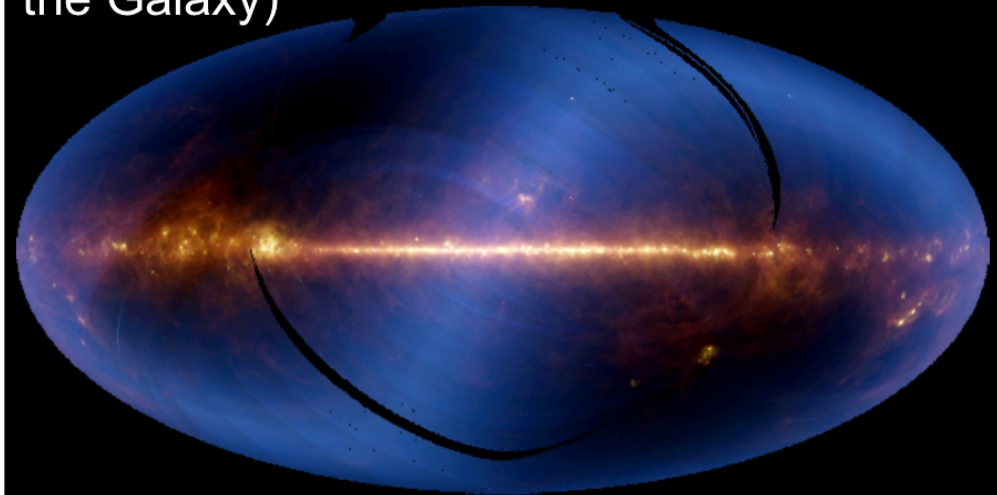

http://coolcosmos.ipac.caltech.edu/image_galleries/IRAS/allsky.html

Classical ZLE: a different approach …

Separated in "time domain", for now simply exploiting differences in surveys

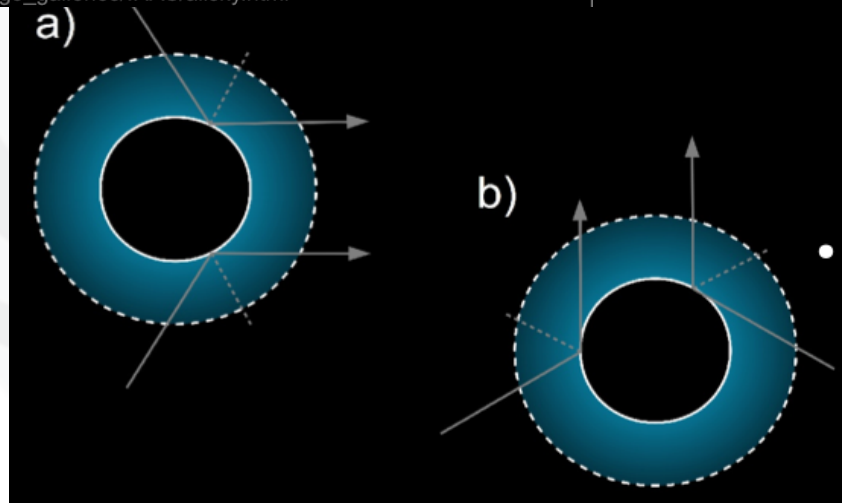

- In successive surveys we observe similar, but different total columns of interplanetary (local) dust (IPD)
- Making differences of successive surveys allows us to remove "contamination", but still be sensitive to the IPD

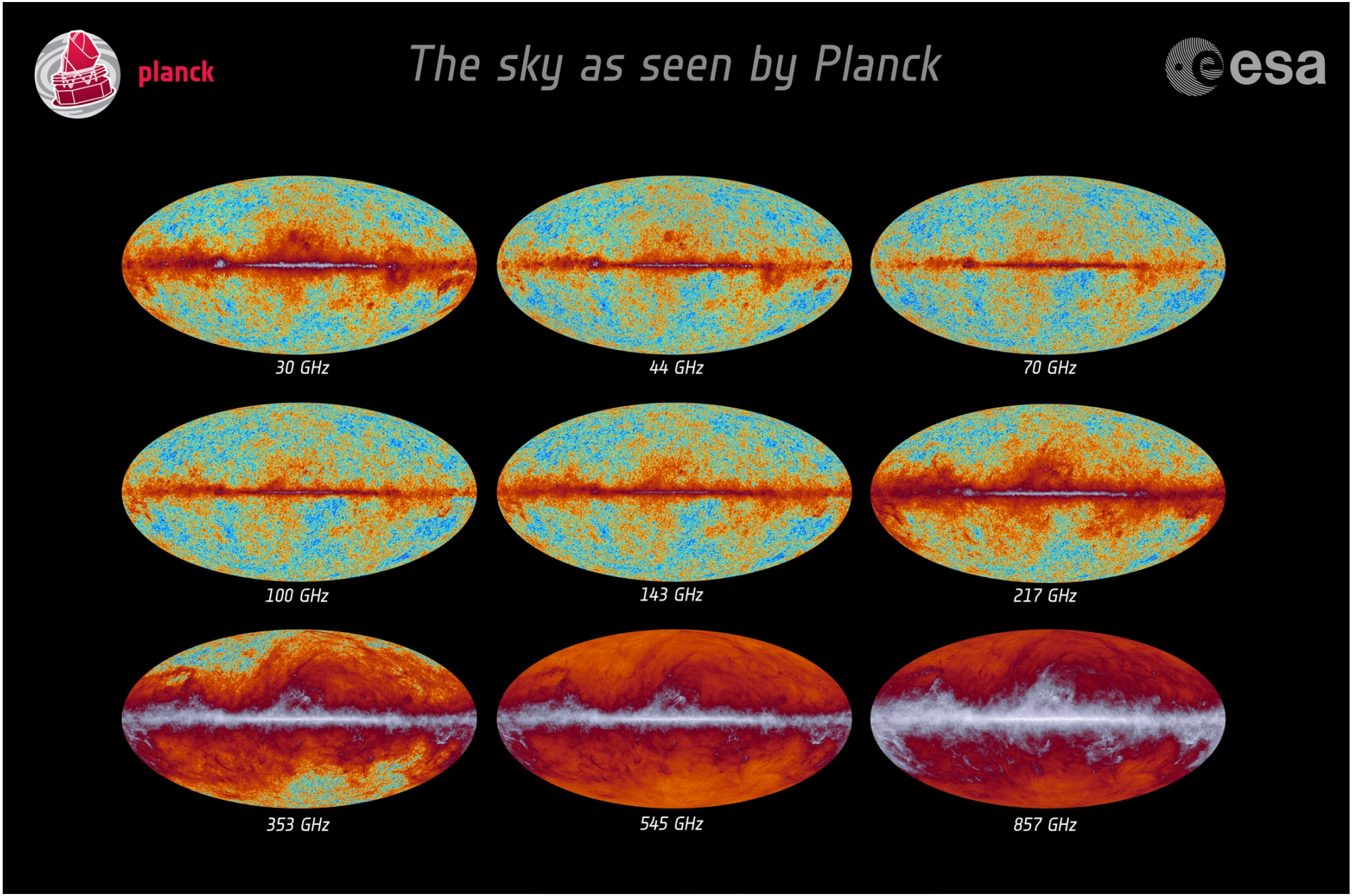
planck
The sky as seen by Planck
esa
30 GHz
44 GHz
70 GHz
100 GHz
143 GHz
217 GHz
353 GHz
545 GHz
857 GHz

PLANCK MICROWAVE SKY

http://spaceinvideos.esa.int/Missions/Planck

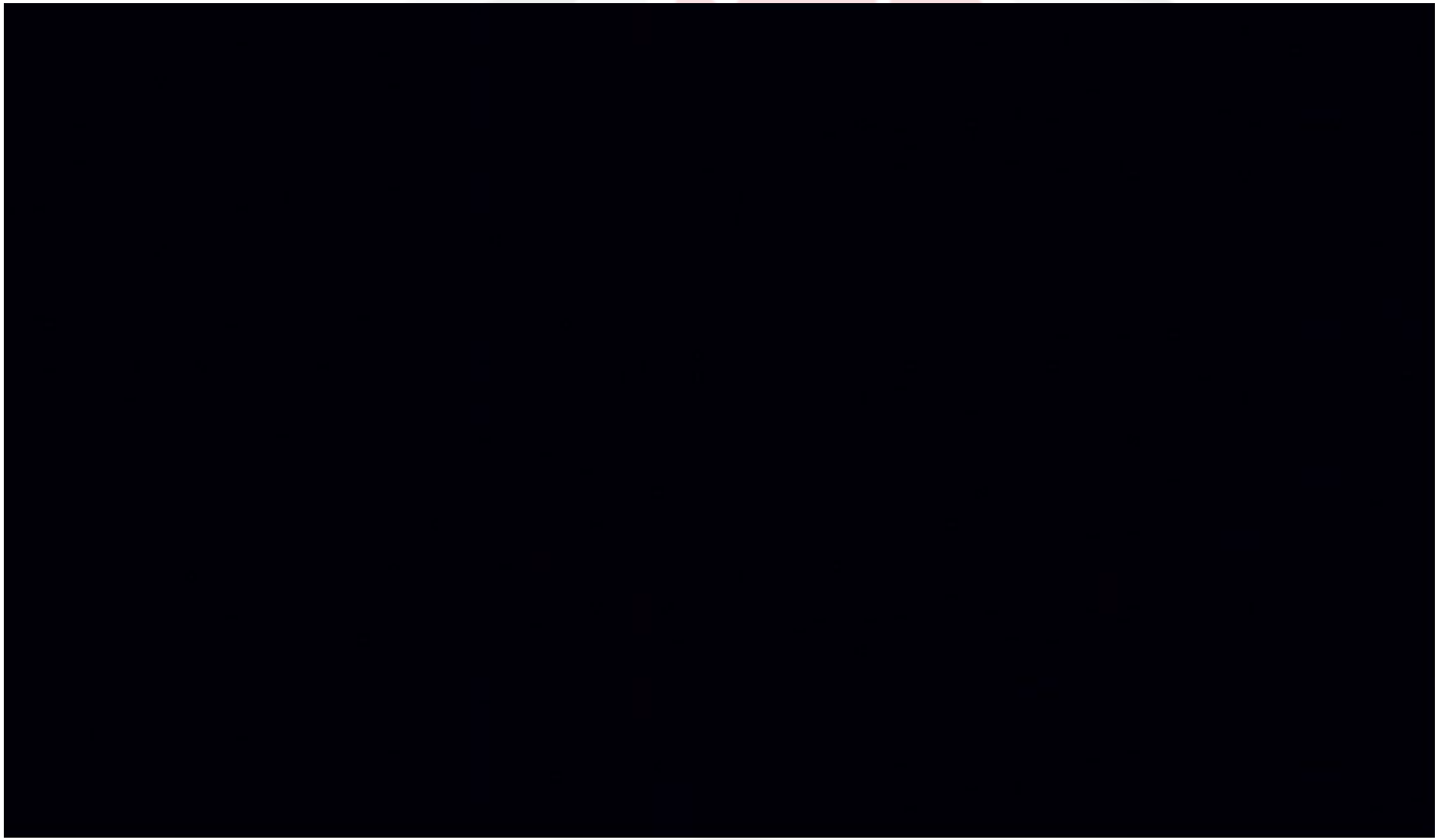

Brief Overview of *Planck* Products

http://www.sciops.esa.int/index.php?project=planck&page=Planck_Legacy_Archive

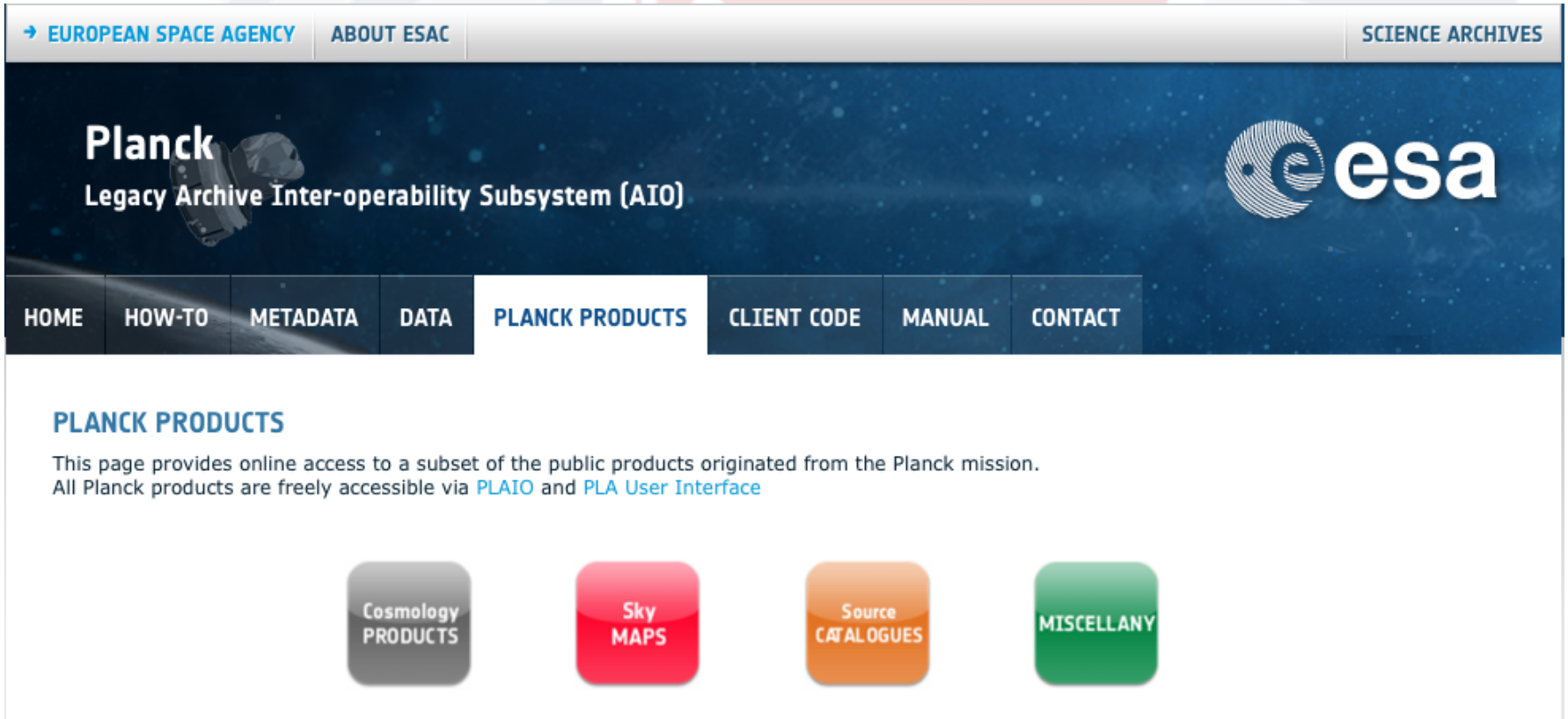

The *Planck* Catalogue (PCCS)

Table 1. PCCS characteristics

Channel	30	44	70	100	143	217	353	545	857
Freq [GHz]	28.4	44.1	70.4	100.0	143.0	217.0	353.0	545.0	857.0
λ [μm]	10561	6807	4260	3000	2098	1382	850	550	350
Beam FWHM[a] [arcmin]	32.38	27.10	13.30	9.65	7.25	4.99	4.82	4.68	4.33
S/N thresholds									
Full sky	4.0	4.0	4.0	4.6	4.7	4.8	...	...	...
Extragactic zone[b]	...	...	...	...	...	...	4.9	4.7	4.9
Galactic zone[b]	...	...	...	...	...	...	6.0	7.0	7.0
Number of sources									
Full sky	1256	731	939	3850	5675	16070	13613	16933	24381
$\|b\| > 30°$	572	258	332	845	1051	1901	1862	3738	7536
Flux densities									
Minimum[c] [mJy]	461	825	566	266	169	149	289	457	658
90 % completeness [mJy]	575	1047	776	300	190	180	330	570	680
Uncertainty [mJy]	109	198	149	61	38	35	69	118	166
Position uncertainty[d] [arcmin]	1.8	2.1	1.4	1.0	0.7	0.7	0.8	0.5	0.4

[a] FEBeCoP band-averaged effective beam. This table shows the exact values that were adopted for the PCCS. For HFI channels, these are the FWHM of the mean best-fit Gaussian. For the LFI channels, we use $FWHM_{\rm eff} = \sqrt{\frac{\Omega_{\rm eff}}{2\pi} 8 \log 2}$, where $\Omega_{\rm eff}$ is the FEBeCoP band-averaged effective solid angle (see Planck Collaboration IV 2013 and Planck Collaboration VII 2013 for a full description of the *Planck* beams). When we constructed the PCCS for the LFI channels we used a value of the effective FWHM slightly different (by $\ll 1\%$) of the final values specified in the Planck Collaboration IV (2013) paper. This small correction will be made in later versions of the catalogue.

[b] The Galactic and extragalactic zones are defined in Sect. 2.3.

[c] Minimum flux density of the catalogue at $|b| > 30°$ after excluding the faintest 10 % of sources.

[d] Positional uncertainty derived by comparison with PACO sample (Massardi et al. 2011; Bonavera et al. 2011; Bonaldi et al. 2013) up to 353 GHz and with *Herschel* samples in the other channels (see Sect. 3.2.3 for more details).

PCCS: Characteristics

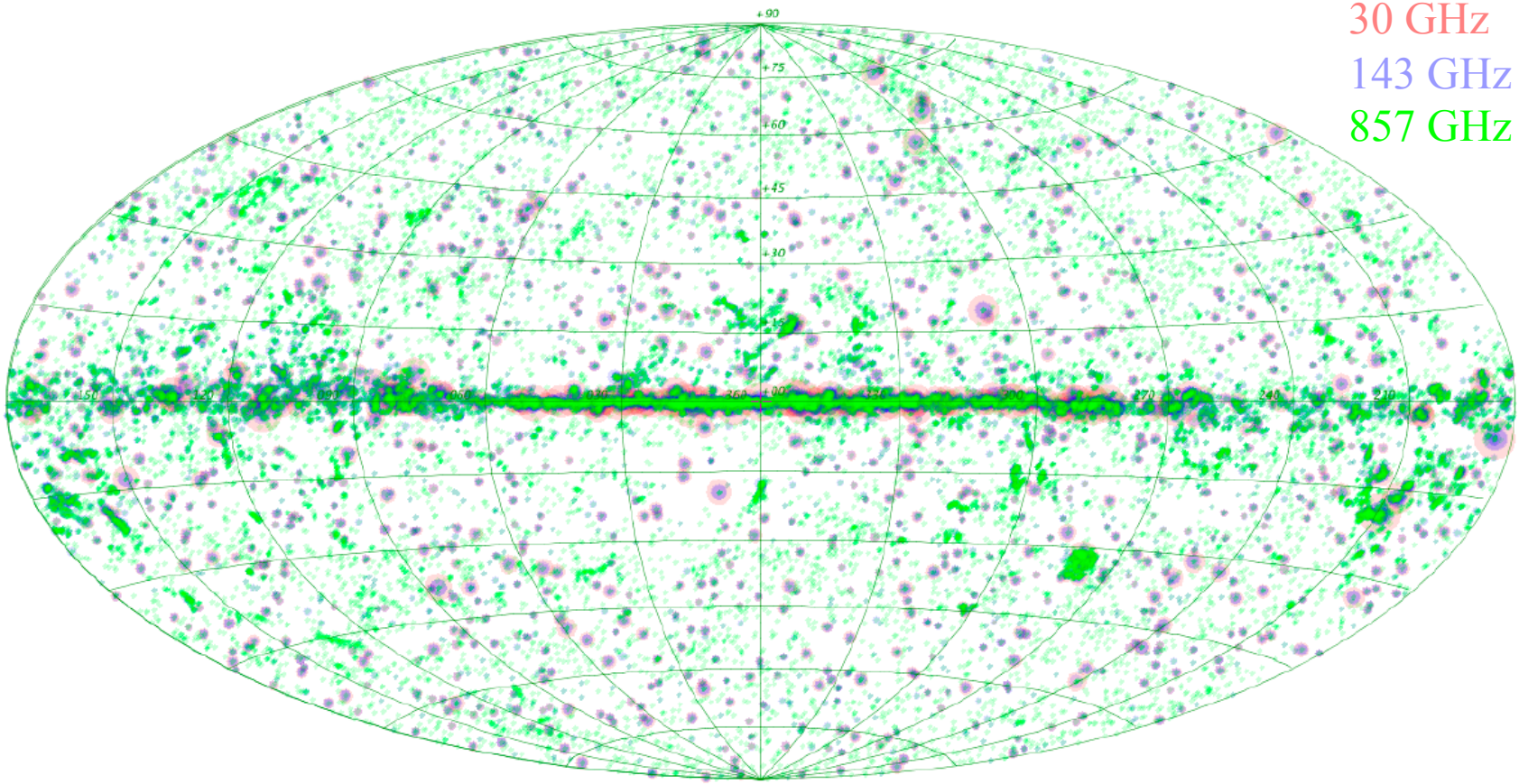

Many of the Planck PCCS sources can be associated with stars with dust shells, stellar cores, radio galaxies, blazars, infrared luminous galaxies and Galactic interstellar medium features.

As expected, the high frequency channels (545 and 857 GHz) are dominated (> 90 %) by dusty galaxies and the low frequency ones are dominated (> 95 %) by synchrotron sources.

The *Planck* Catalogue (PCCS)

…but the PCCS has not been analyzed, yet! (future papers → 2014-15)

PCCS: Sensitivity

- PCCS is the most complete all-sky catalogue in the microwave band.

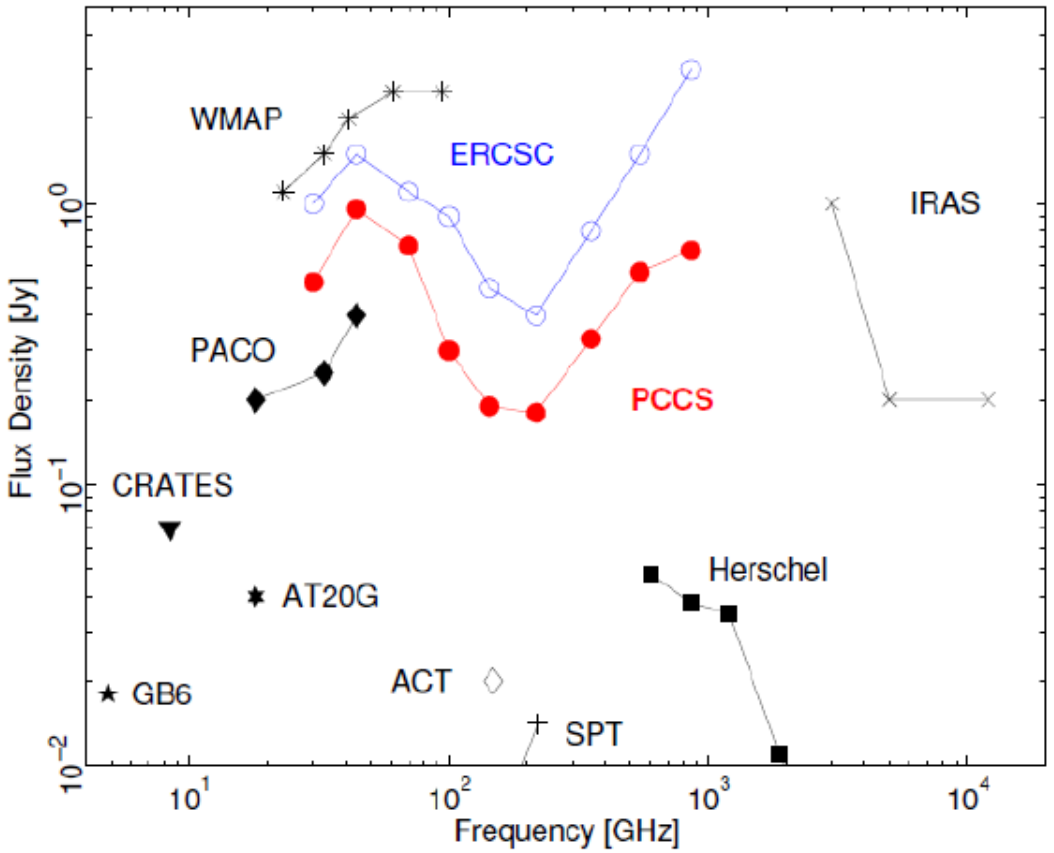

Thermal and kinetic Sunyaev-Zeldovich (SZ) effect towards galaxy clusters

The scattering of CMB photons from hot electrons in galaxies and clusters of galaxies produces a frequency dependent change in the CMB brightness (Sunyaev & Zeldovich '72, Rephaeli '95 [1,2]):

- ✧ hot electron gas is globally at rest with respect to the observer → thermal SZ effect
- ✧ bulk peculiar motion, Vr, of the hot electron gas → kinetic SZ effect

In the Rayleigh-Jeans (RJ) region:

- ➢ thermal SZ effect → decrement of the surface brightness towards the cluster
- ➢ kinetic SZ effect → decrement or an increment depending on the direction of the cluster velocity with respect to the observer

They can be separated through multi-frequency observations on a wide frequency range.

Planck 2013 results. XXIX. Planck catalogue of Sunyaev–Zeldovich sources

- The catalogue contains **1227 entries**, making it over six times the size of the Planck Early SZ (ESZ) sample and the largest SZ-selected deepest all-sky cluster ccatalogue to date.
- It contains **861 confirmed** clusters: 178 have been confirmed as clusters, mostly through follow-ups, and a further 683 are previously-known.
- 366 are cluster candidates: three classes according to the quality of evidence that they are likely to be true clusters.
- z to ≅ 1, broadest **range from (0.1 to 1.6) × 10^{15} $M_{\odot}$**.
- **Confirmation** of cluster candidates through comparison with existing surveys or cluster catalogues, catalogue statistical characterization in terms of completeness and statistical reliability. **Validation** process through additional information.
- This gives an ensemble of **813 cluster redshifts**, and for all these *Planck* clusters we also include a **mass** estimated from a newly-proposed SZ-mass proxy.
- Refined measure of the **SZ Compton parameter** for the clusters with X-ray counter -parts, **X-ray flux** for all the *Planck* clusters not previously detected in X-ray surveys.

Mollweide projection with the Galactic plane horizontal and the Milky Way centre in the middle, of the
1227 Planck clusters and candidates across the sky (red thick dots). Masked point-sources (black thin dots), Magellanic clouds (large black areas), Galactic mask, covering a total of 16.3% of the sky and used by the SZ-finder algorithms to detect SZ sources.

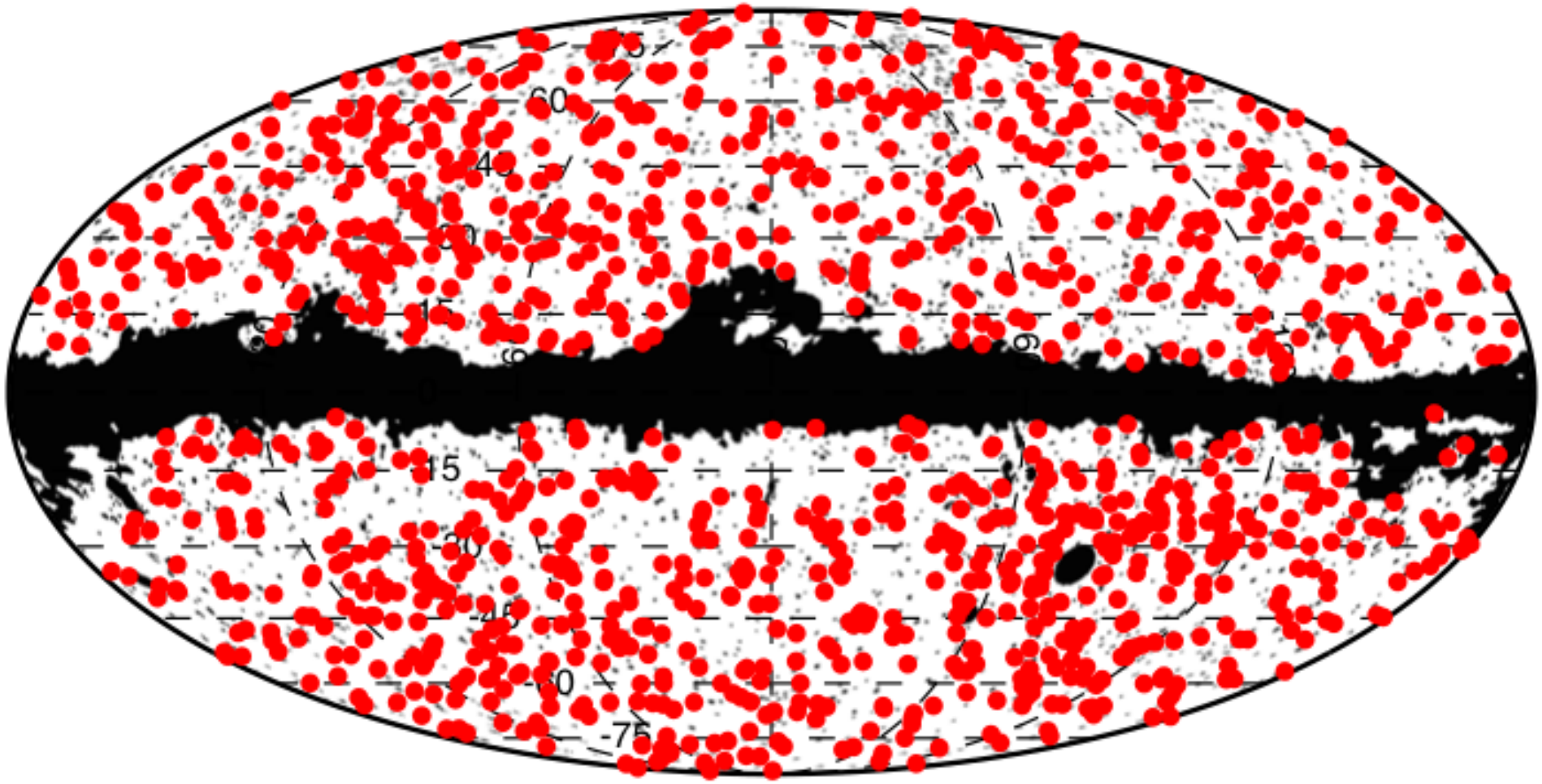

The CMB seen by *Planck* & its cosmological implications

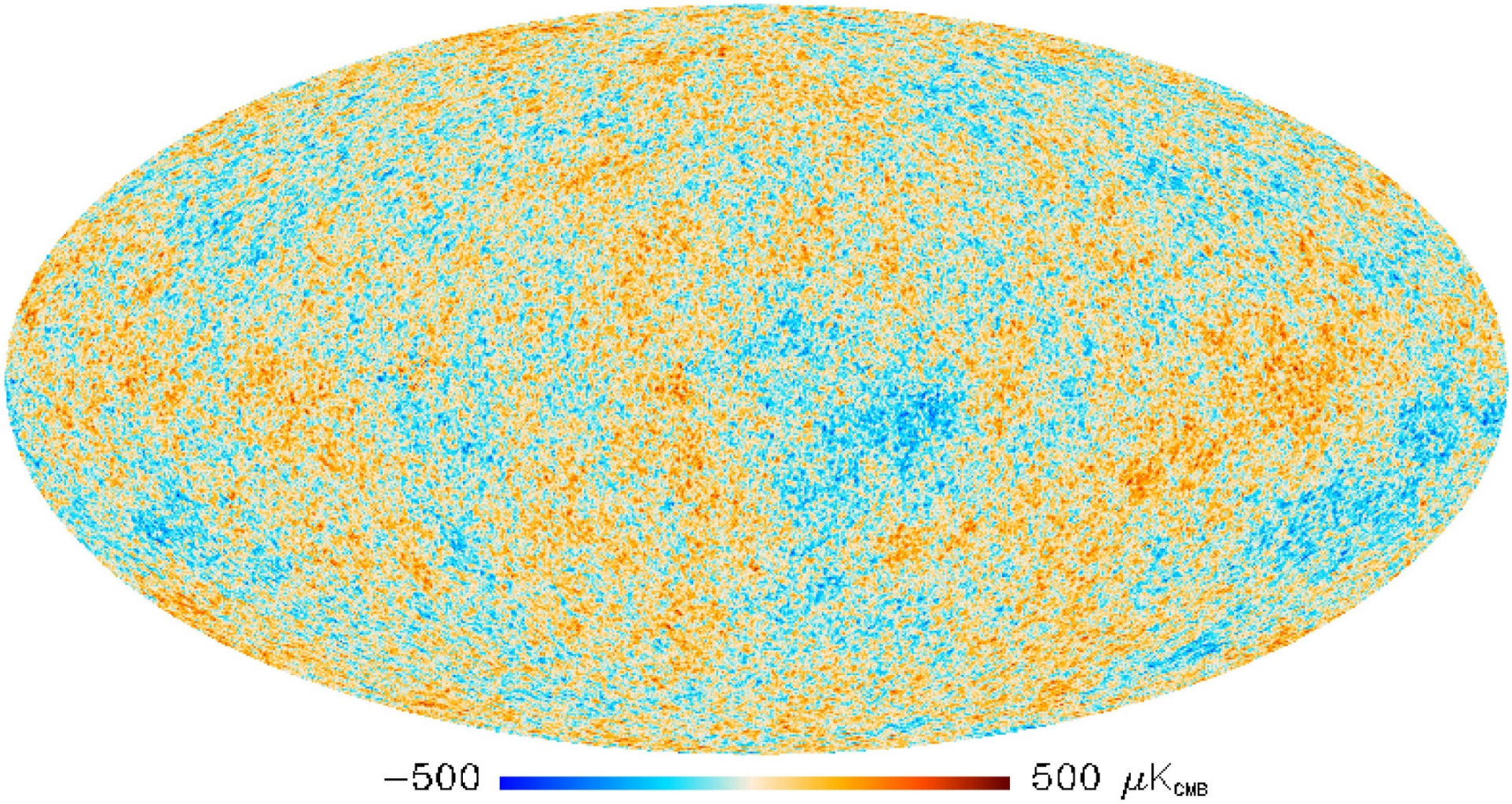

CMB ANISOTROPIES ARE ANALYZED IN A STATISTICAL WAY

$$\Delta T(\vec{x},\hat{n},\tau) = \Sigma_{l=1}^{\infty}\Sigma_{m=-l}^{l} a_{lm}(\vec{x},\tau)Y_{lm}(\hat{n})$$

THE ANGULAR POWER SPECTRUM

$$C_l = \frac{1}{2l+1}\Sigma_m \langle a_{lm}^* a_{lm}\rangle$$

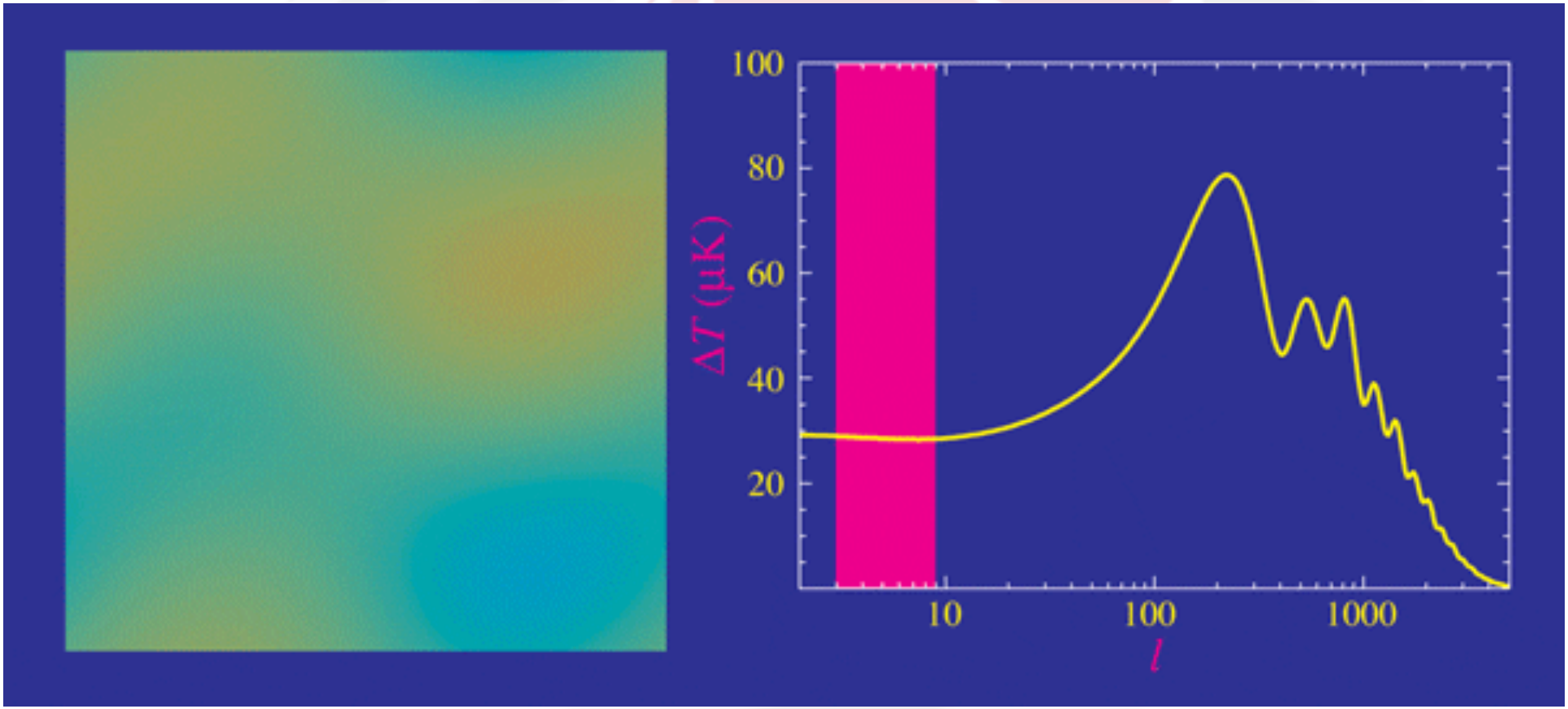

Waine Hu http://background.uchicago.edu/~whu/metaanim.html

APS DEPENDENCE ON COSMOLOGICAL PARAMETERS

***Planck*: a single experiment spanning a wide multipole range!**

Theta → first peak position

Baryon Density → height difference between even and odd peaks

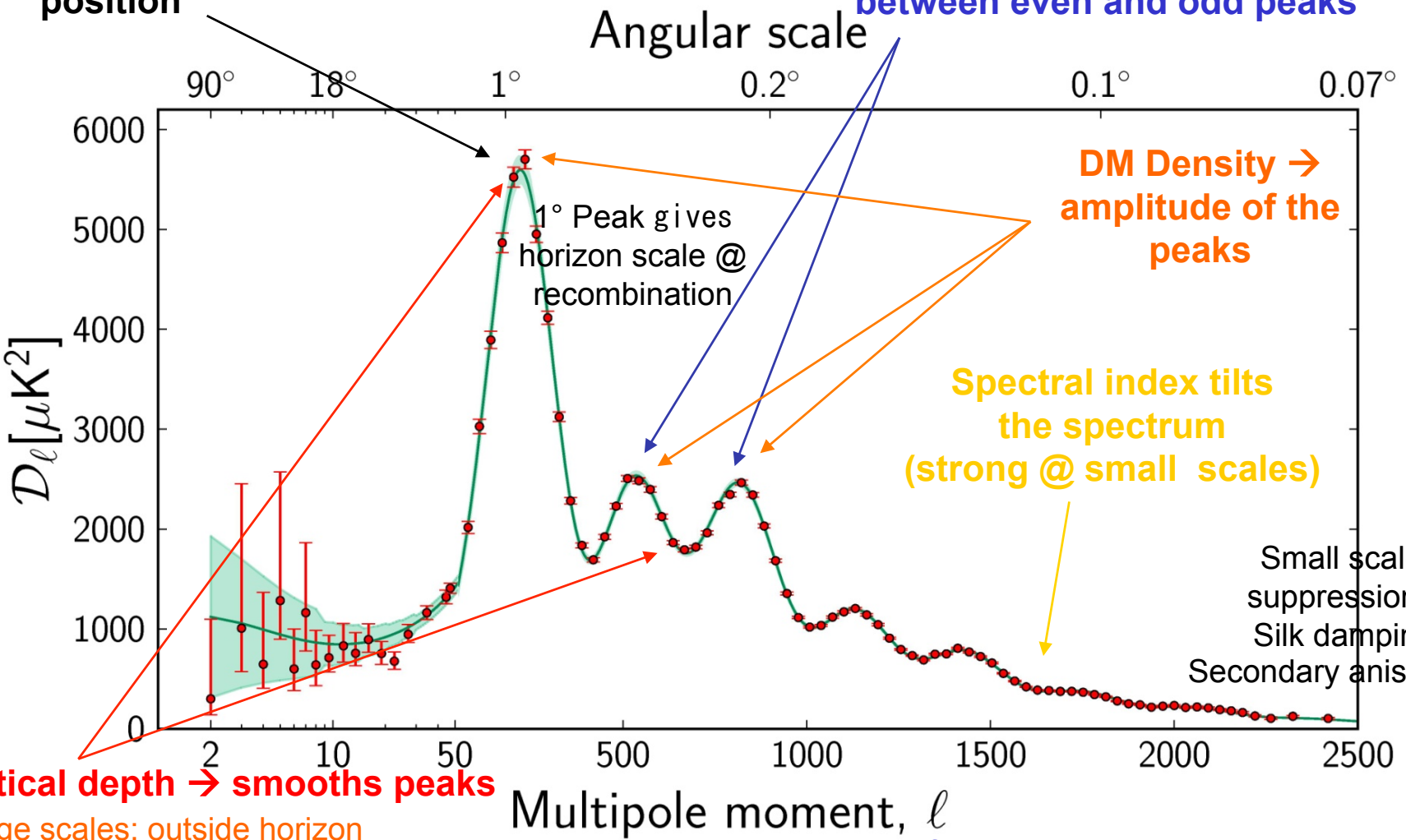

Optical depth → smooths peaks

Large scales: outside horizon @ recombination – only gravity

Intermediate scales: photon-baryon fluid acoustic oscillations - DM potential well vs radiation pressure

PLANCK COSMOLOGICAL PARAMETERS: ΛCDM model

	Planck+WP		*Planck*+WP+highL		*Planck*+lensing+WP+highL		*Planck*+WP+highL+BAO	
Parameter	Best fit	68% limits	Best fit	68% limits	Best fit	68% limits	Best fit	68% limits
$\Omega_b h^2$	0.022032	0.02205 ± 0.00028	0.022069	0.02207 ± 0.00027	0.022199	0.02218 ± 0.00026	0.022161	0.02214 ± 0.00024
$\Omega_c h^2$	0.12038	0.1199 ± 0.0027	0.12025	0.1198 ± 0.0026	0.11847	0.1186 ± 0.0022	0.11889	0.1187 ± 0.0017
$100\theta_{MC}$	1.04119	1.04131 ± 0.00063	1.04130	1.04132 ± 0.00063	1.04146	1.04144 ± 0.00061	1.04148	1.04147 ± 0.00056
τ	0.0925	$0.089^{+0.012}_{-0.014}$	0.0927	$0.091^{+0.013}_{-0.014}$	0.0943	$0.090^{+0.013}_{-0.014}$	0.0952	0.092 ± 0.013
n_s	0.9619	0.9603 ± 0.0073	0.9582	0.9585 ± 0.0070	0.9624	0.9614 ± 0.0063	0.9611	0.9608 ± 0.0054
$\ln(10^{10} A_s)$	3.0980	$3.089^{+0.024}_{-0.027}$	3.0959	3.090 ± 0.025	3.0947	3.087 ± 0.024	3.0973	3.091 ± 0.025
Ω_Λ	0.6817	$0.685^{+0.018}_{-0.016}$	0.6830	$0.685^{+0.017}_{-0.016}$	0.6939	0.693 ± 0.013	0.6914	0.692 ± 0.010
σ_8	0.8347	0.829 ± 0.012	0.8322	0.828 ± 0.012	0.8271	0.8233 ± 0.0097	0.8288	0.826 ± 0.012
z_{re}	11.37	11.1 ± 1.1	11.38	11.1 ± 1.1	11.42	11.1 ± 1.1	11.52	11.3 ± 1.1
H_0	67.04	67.3 ± 1.2	67.15	67.3 ± 1.2	67.94	67.9 ± 1.0	67.77	67.80 ± 0.77
Age/Gyr	13.8242	13.817 ± 0.048	13.8170	13.813 ± 0.047	13.7914	13.794 ± 0.044	13.7965	13.798 ± 0.037
$100\theta_*$	1.04136	1.04147 ± 0.00062	1.04146	1.04148 ± 0.00062	1.04161	1.04159 ± 0.00060	1.04163	1.04162 ± 0.00056
r_{drag}	147.36	147.49 ± 0.59	147.35	147.47 ± 0.59	147.68	147.67 ± 0.50	147.611	147.68 ± 0.45

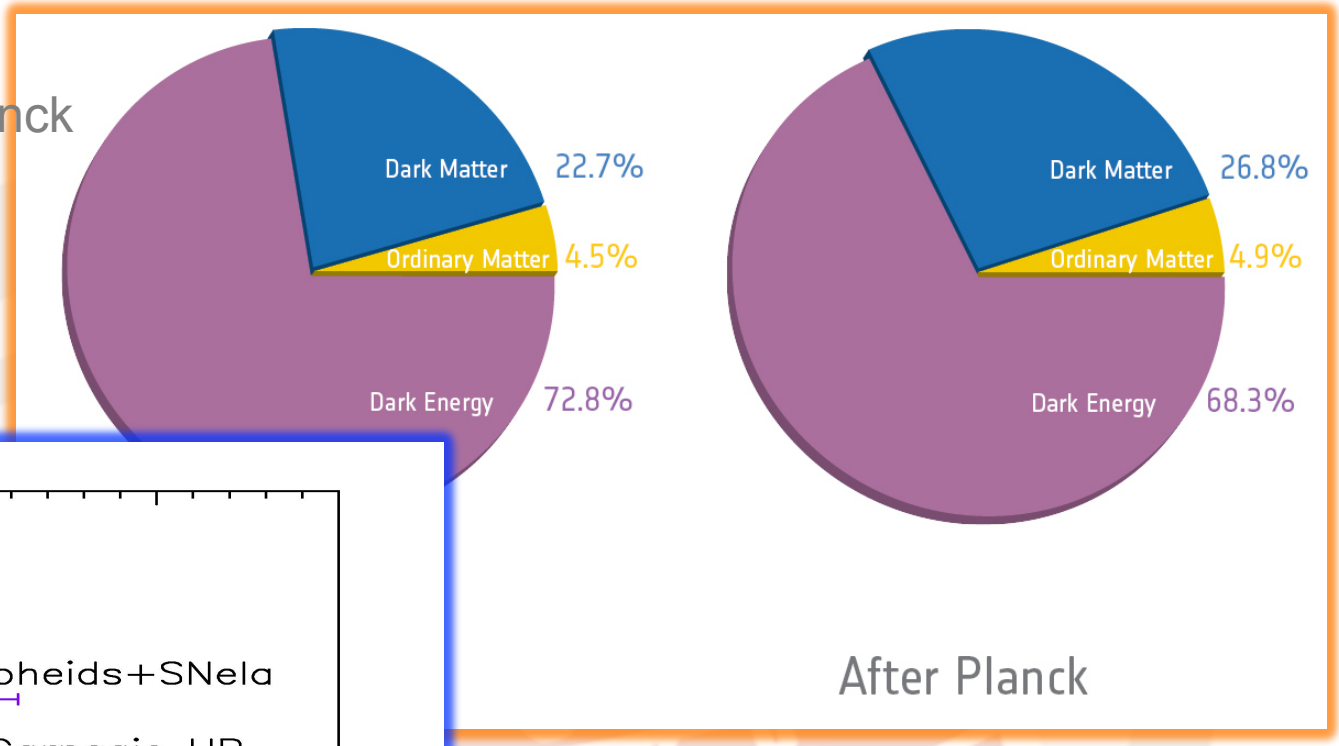

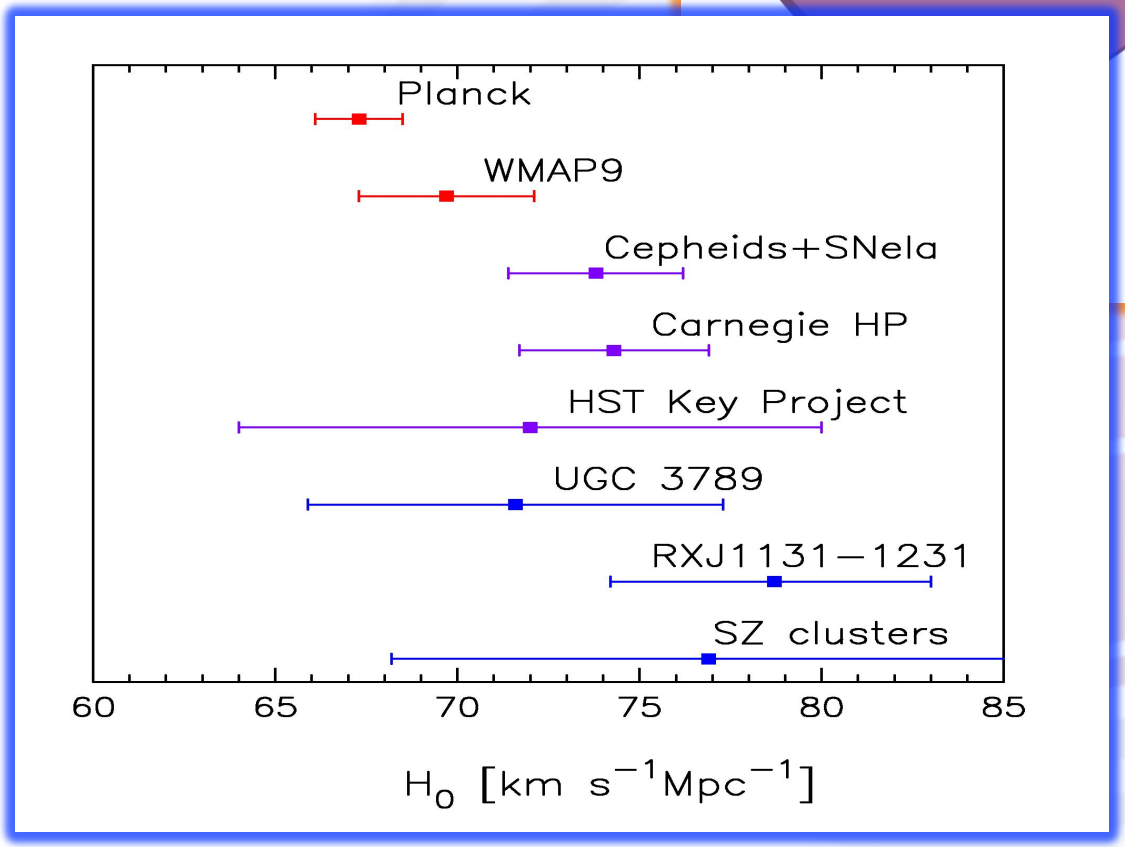

Types of energy densities & Universe age

Slide from Francois Bouchet
Inflation has a few variants...

- assisted brane inflation
- anomaly-induced inflation
- assisted inflation
- assisted chaotic inflation
- B-inflation
- boundary inflation
- brane inflation
- brane-assisted inflation
- brane gas inflation
- brane-antibrane inflation
- braneworld inflation
- Brans-Dicke chaotic inflation
- Brans-Dicke inflation
- bulky brane inflation
- chaotic inflation
- chaotic hybrid inflation
- chaotic new inflation
- Chromo-Natural Inflation
- D-brane inflation
- D-term inflation
- dilaton-driven inflation
- dilaton-driven brane inflation
- double inflation
- double D-term inflation
- dual inflation
- dynamical inflation
- dynamical SUSY inflation
- S-dimensional assisted inflation
- eternal inflation
- extended inflation
- extended open inflation
- extended warm inflation
- extra dimensional inflation
- ...

- F-term inflation
- F-term hybrid inflation
- false-vacuum inflation
- false-vacuum chaotic inflation
- fast-roll inflation
- first-order inflation
- gauged inflation
- Ghost inflation
- Hagedorn inflation
- higher-curvature inflation
- hybrid inflation
- Hyper-extended inflation
- induced gravity inflation
- intermediate inflation
- inverted hybrid inflation
- Power-law inflation
- K-inflation
- Super symmetric inflation

- Quintessential inflation
- Roulette inflation
- curvature inflation
- Natural inflation
- Warm natural inflation
- Super inflation
- Super natural inflation
- Thermal inflation
- Discrete inflation
- Polarcap inflation
- Open inflation
- Topological inflation
- Multiple inflation
- Warm inflation
- Stochastic inflation
- Generalised assisted inflation
- Self-sustained inflation
- Graduated inflation
- Local inflation
- Singular inflation
- Slinky inflation
- Locked inflation
- Elastic inflation
- Mixed inflation
- Phantom inflation
- Non-commutative inflation
- Tachyonic inflation
- Tsunami inflation
- Lambda inflation
- Steep inflation
- Oscillating inflation
- Mutated hybrid inflation
- Inhomogeneous inflation
- ...

Model	Parameter	*Planck*+WP	*Planck*+WP+lensing	*Planck* + WP+high-ℓ	*Planck*+WP+BAO
ΛCDM + tensor	n_s	0.9624 ± 0.0075	0.9653 ± 0.0069	0.9600 ± 0.0071	$0.9643 + 0.0059$
	$r_{0.002}$	< 0.12	< 0.13	< 0.11	< 0.12
	$-2\Delta \ln \mathcal{L}_{\rm max}$	0	0	0	-0.31

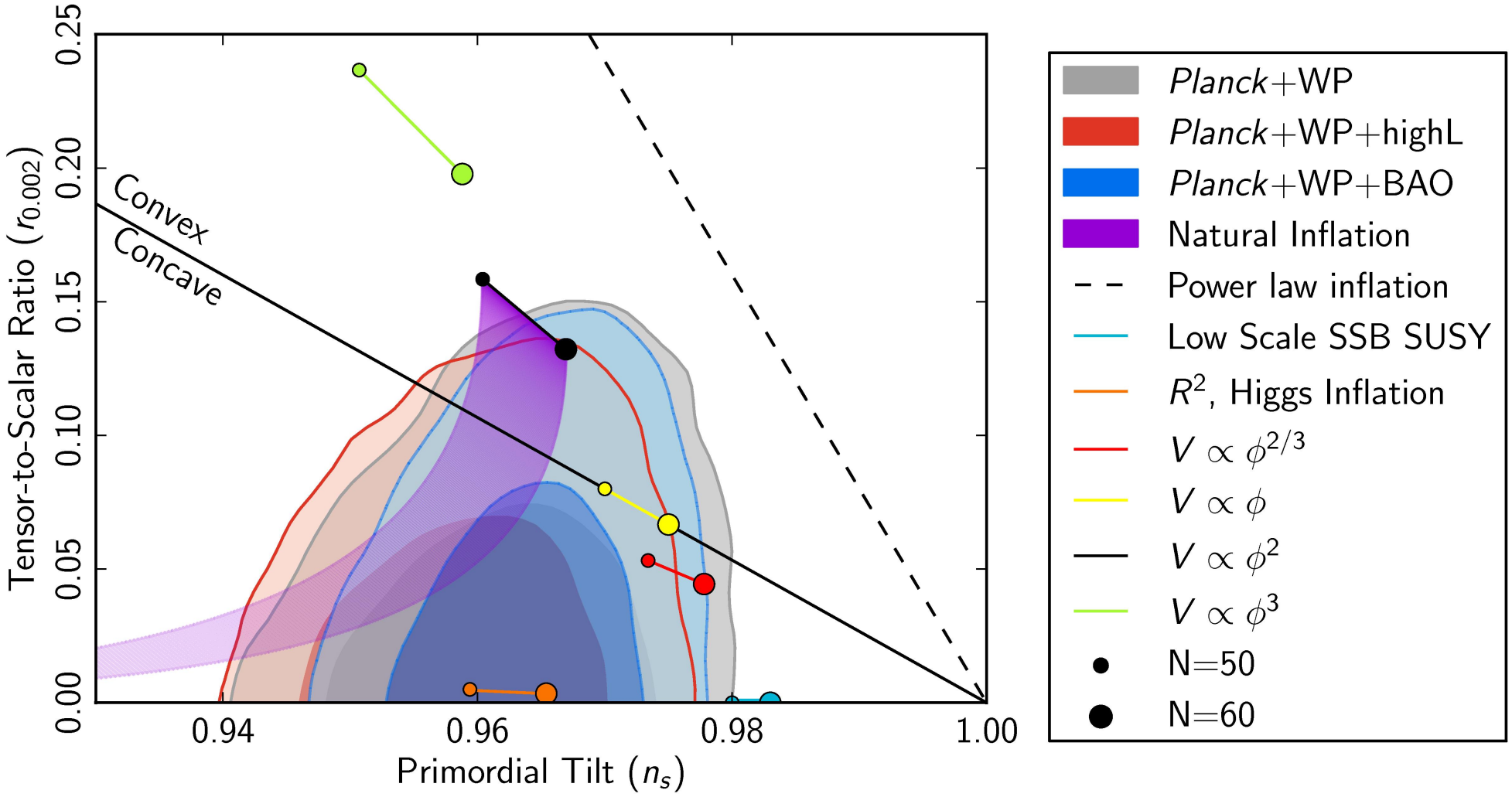

Robustness n_s - r

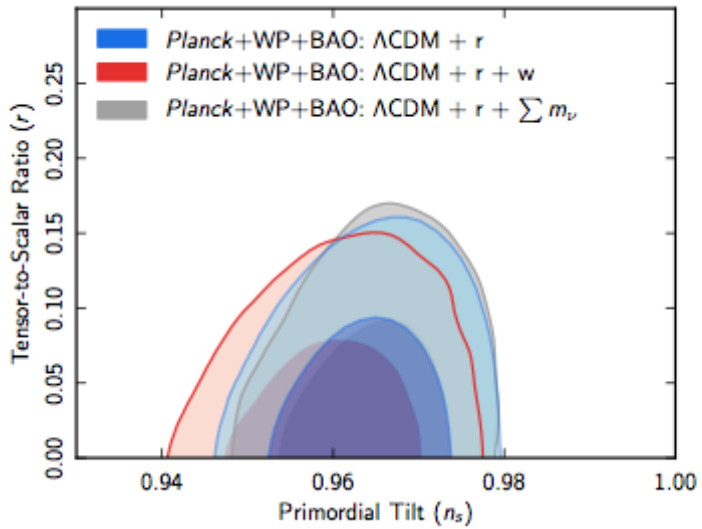

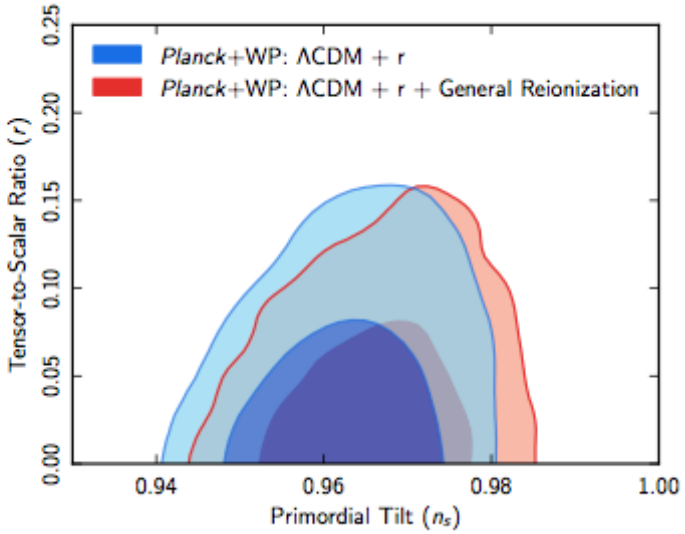

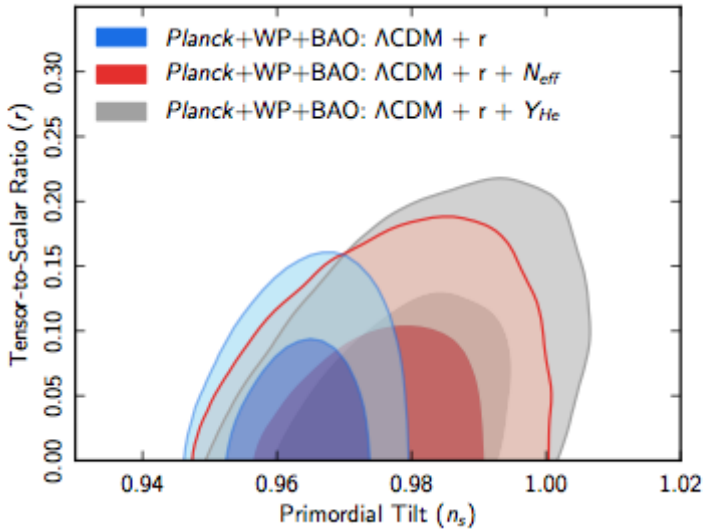

RUNNING OF THE SPECTRAL INDEX

$$\mathcal{P}_{\mathcal{R}}(k) = A_{\rm s}\left(\frac{k}{k_*}\right)^{n_{\rm s}-1+\frac{1}{2}\,{\rm d}n_{\rm s}/{\rm d}\ln k\,\ln(k/k_*)+\frac{1}{6}\,{\rm d}^2 n_{\rm s}/{\rm d}\ln k^2(\ln(k/k_*))^2+\cdots}$$

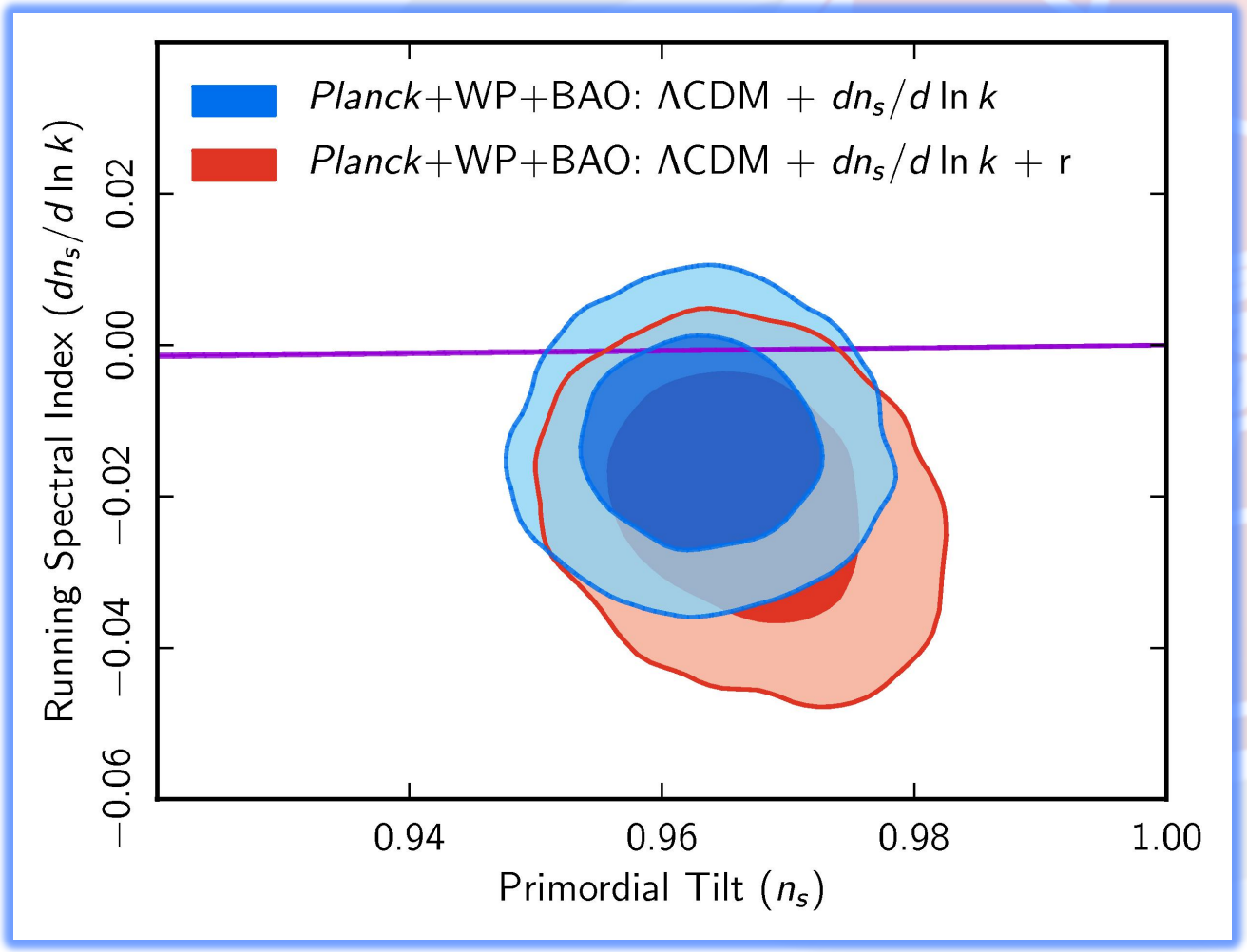

COMPATIBLE WITH ZERO RUNNING

(WITH A PREFERENCE FOR NEGATIVE VALUES)

Lack of power at low multipoles

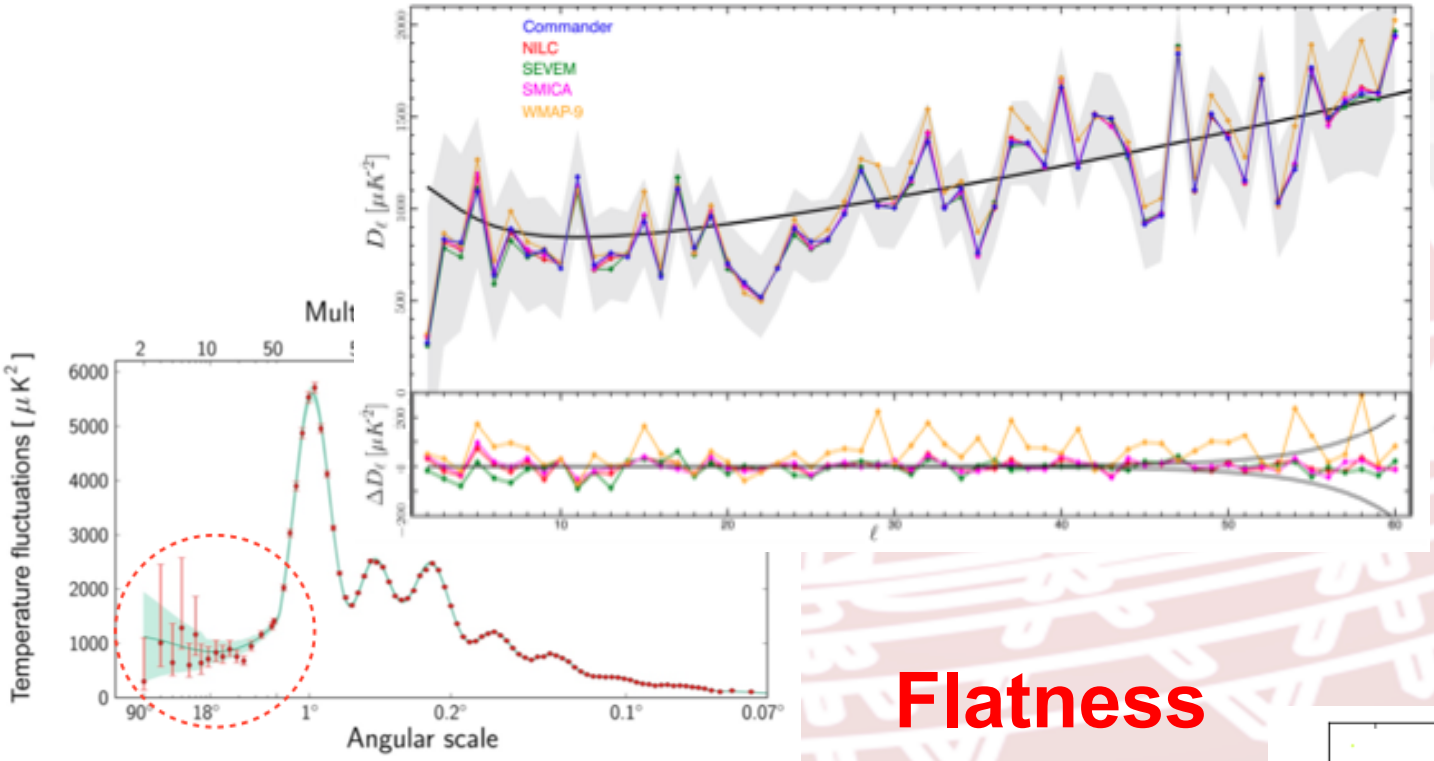

+ tensors

Ω_K=-0.0006±0.0069
r < 0.13 *(95%; Planck+WP+BAO)*

+ running

(Ω_K + r + $dn_s/d\ln k$)

Flatness

$$\Omega_K = -0.042^{+0.043}_{-0.048} \quad \textit{(95\%; Planck+WP+highL)}$$

$$\Omega_K = -0.007^{+0.018}_{-0.020} \quad \textit{(95\%; Planck+lensing+WP)}$$

$$\Omega_K = -0.010^{+0.018}_{-0.019} \quad \textit{(95\%; Planck+lensing+WP+highL)}$$

$$\Omega_K = 0.000^{+0.0066}_{-0.0067} \quad \textit{(95\%; Planck+WP+BAO)}$$

$$\Omega_K = -0.0010^{+0.0062}_{-0.0065} \quad \textit{(95\%; Planck+lensing+WP+highL+BAO)}$$

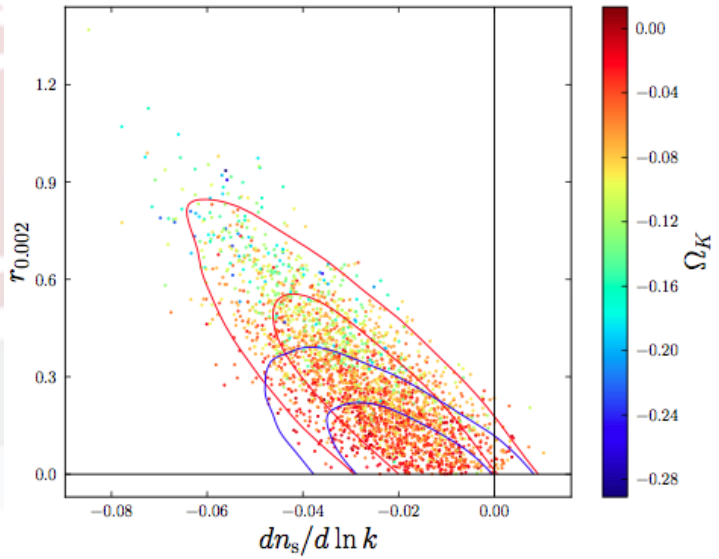

DARK ENERGY

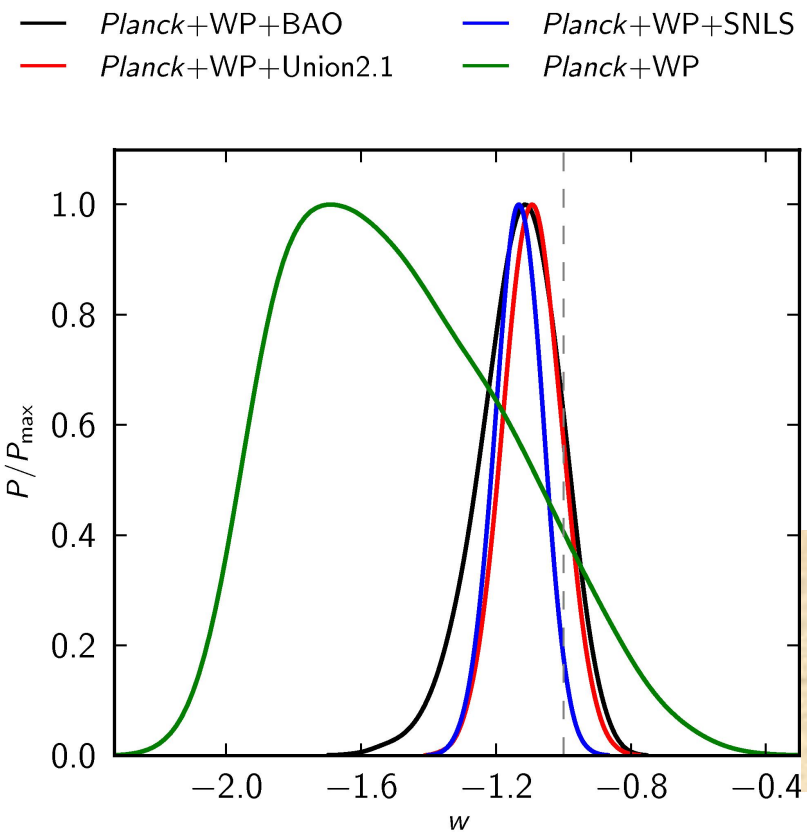

Compatible with a cosmological constant equation of state

$w = -1.13 \pm 0.24$

No need for dynamical DE

REL. NEUTRINOS

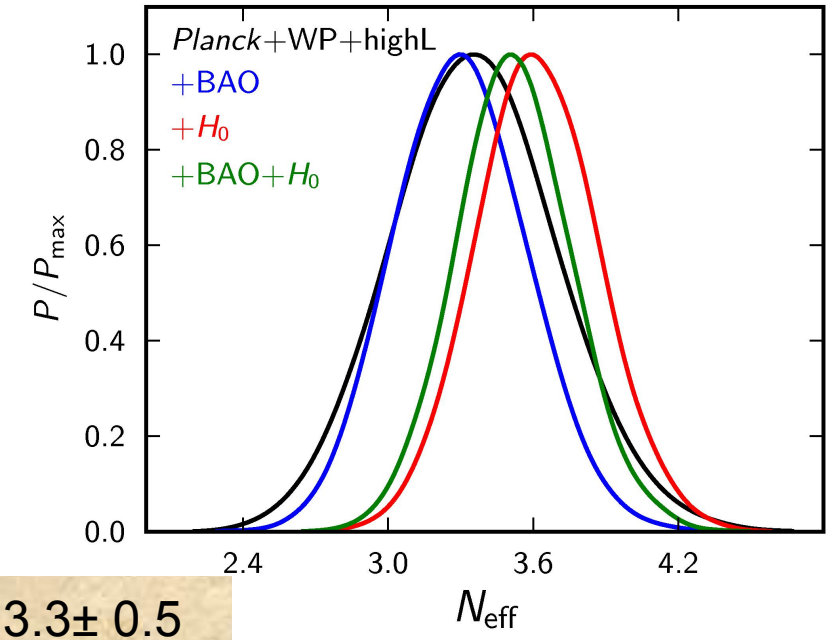

Neff = 3.3± 0.5

compatible with

? standard 3.046

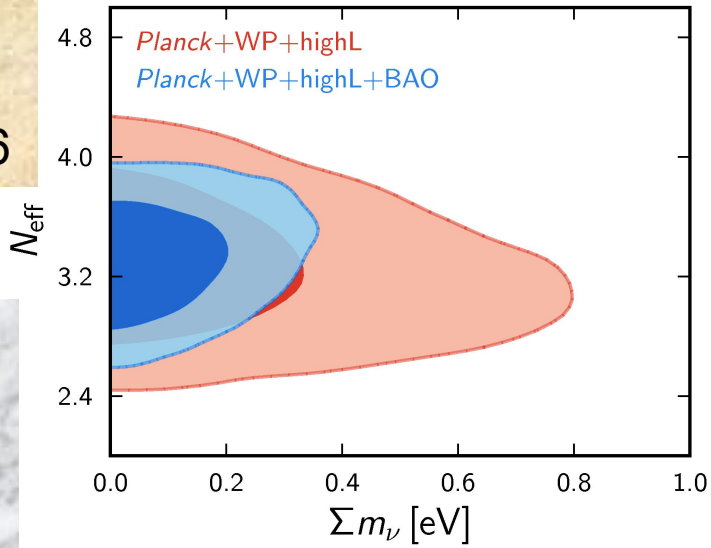

Constraints on neutrino masses:

$\Sigma m_\nu < 0.23 eV$

Non-Gaussianity … mainly through CMB bispectrum

$$B^{m_1 m_2 m_3}_{\ell_1 \ell_2 \ell_3} \equiv \langle a_{\ell_1 m_1} a_{\ell_2 m_2} a_{\ell_3 m_3} \rangle$$

$$= \mathcal{G}^{\ell_1 \ell_2 \ell_3}_{m_1 m_2 m_3} \, b_{\ell_1 \ell_2 \ell_3}$$

Gaunt integrals

$$\mathcal{G}^{\ell_1 \ell_2 \ell_3}_{m_1 m_2 m_3} \equiv \int Y_{\ell_1 m_1}(\hat{\mathbf{n}}) \, Y_{\ell_2 m_2}(\hat{\mathbf{n}}) \, Y_{\ell_3 m_3}(\hat{\mathbf{n}}) \, d^2\hat{\mathbf{n}}$$

$$= h_{\ell_1 \ell_2 \ell_3} \begin{pmatrix} \ell_1 & \ell_2 & \ell_3 \\ m_1 & m_2 & m_3 \end{pmatrix},$$

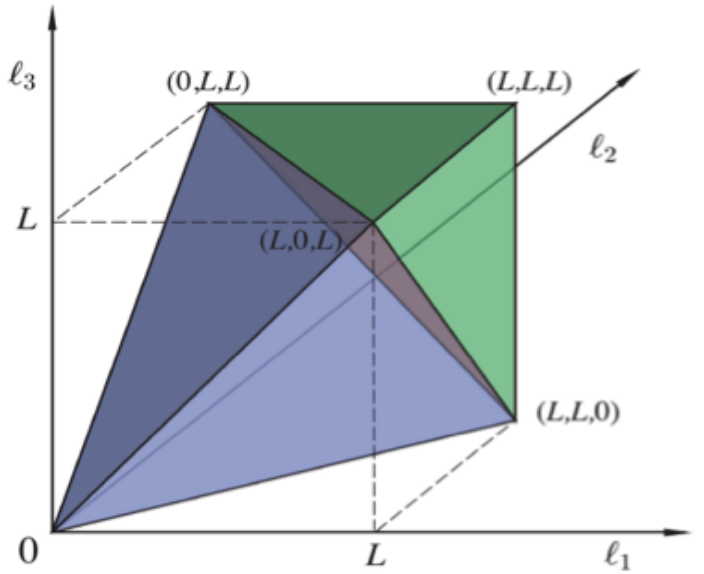

Triangle condition: $\ell_1 \le \ell_2 + \ell_3$ for $\ell_1 \ge \ell_2, \ell_3$, +perms.

Parity condition: $\ell_1 + \ell_2 + \ell_3 = 2n, \quad n \in \mathbb{N},$

Resolution: $\ell_1, \ell_2, \ell_3 \le \ell_{\max}, \quad \ell_1, \ell_2, \ell_3 \in \mathbb{N}.$

(1) Multiple fields (local models, non-linearities develop outside horizon)

(2) Non-canonical kinetic term of quantum fields (higher derivative interactions; Dirac-Born-Infeld, K-inflation)

(3) Non-vacuum initial conditions

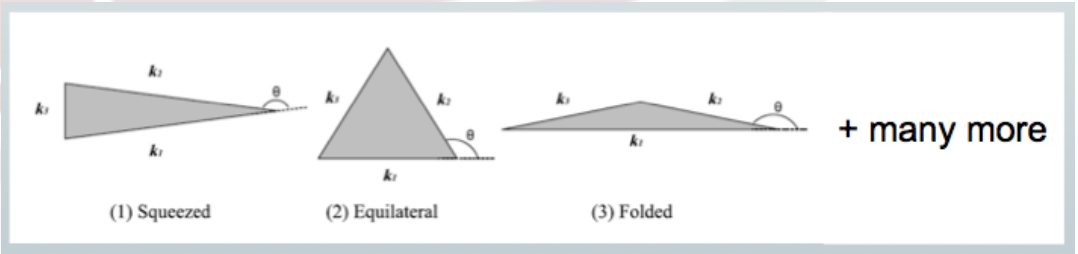

f_{NL} from *Planck* data

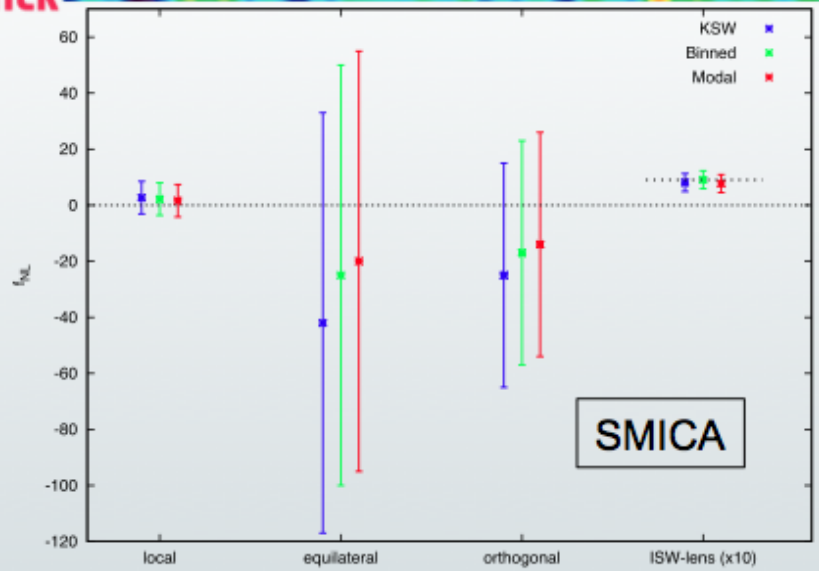

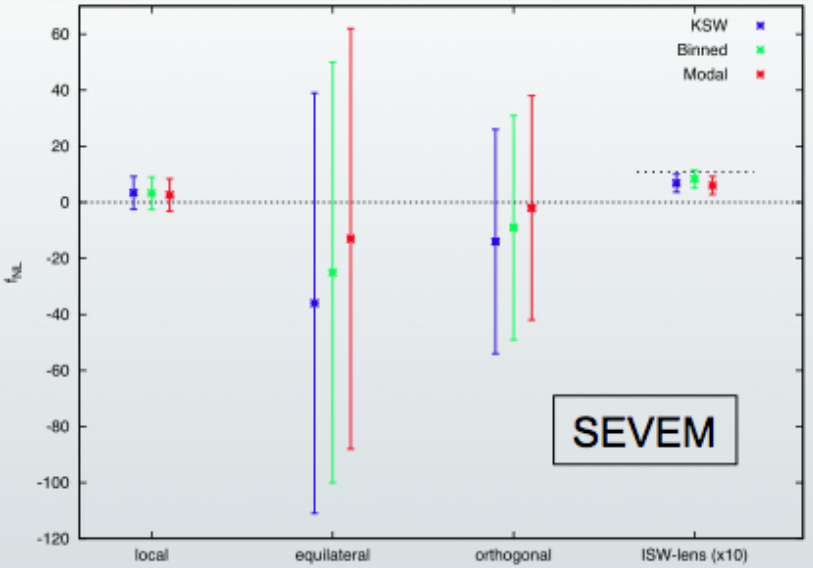

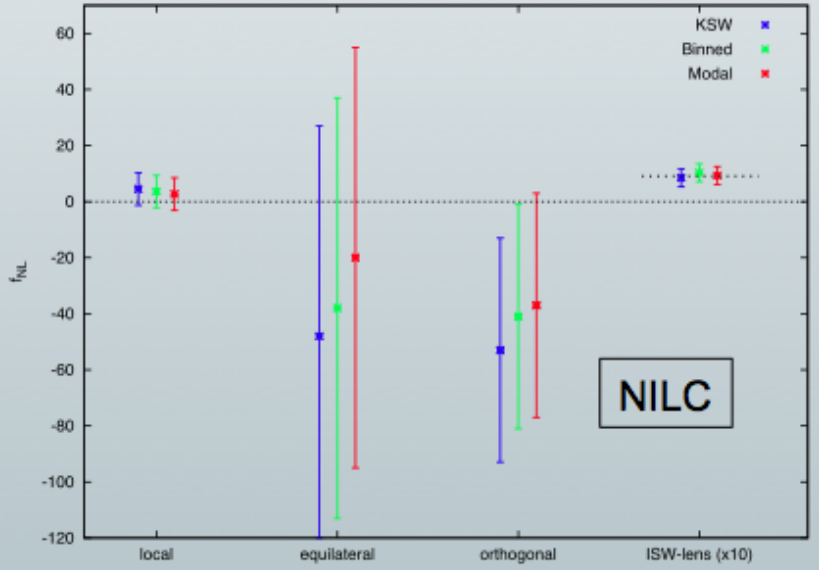

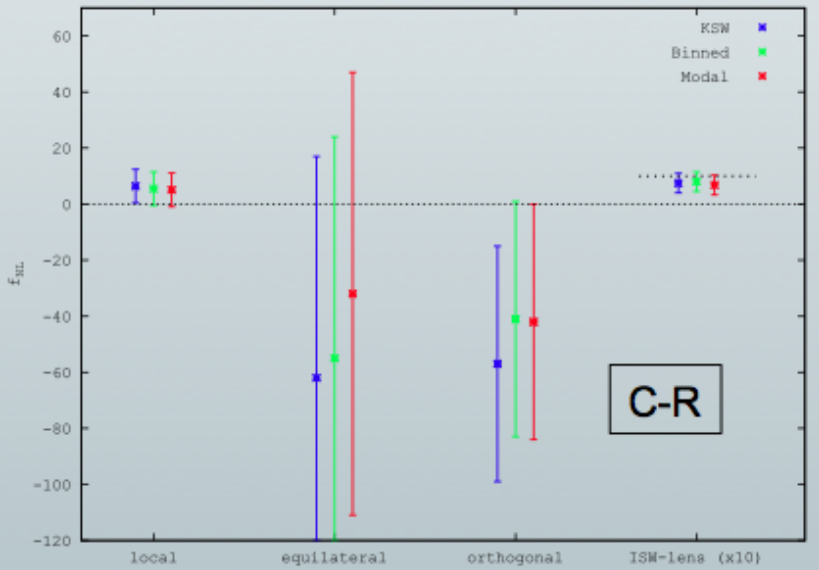

Non-Gaussianity summary

- We have **detected the ISW-lensing bispectrum**, as expected in ΛCDM scenario.
- We have derived **constraints on early-Universe scenarios that generate primordial NG**, including general single-field models of inflation, excited initial states (non-Bunch-Davies vacua), and directionally-dependent vector models.
- Initial survey of scale-dependent feature and resonance models.

  These results bound both general single-field and multi-field model parameter ranges, such as the speed of sound,

  $c_s \geq 0.02$ (95% CL), in an effective field theory parametrization ($c_s \geq 0.07$ for DBI inflation),

  and the curvaton decay fraction $r_D \geq 0.15$ (95% CL).
- **The simplest inflation models (single-field slow-roll, standard kinetic term, BD initial vacuum state) are favoured by *Planck* data.**
- Multi-field models are not ruled out but also not detected.
- Ekpyrotic/cyclic models either ruled our or under severe pressure.
- Taken together, these constraints represent the **highest precision tests** to date of physical mechanisms for the origin of cosmic structure.

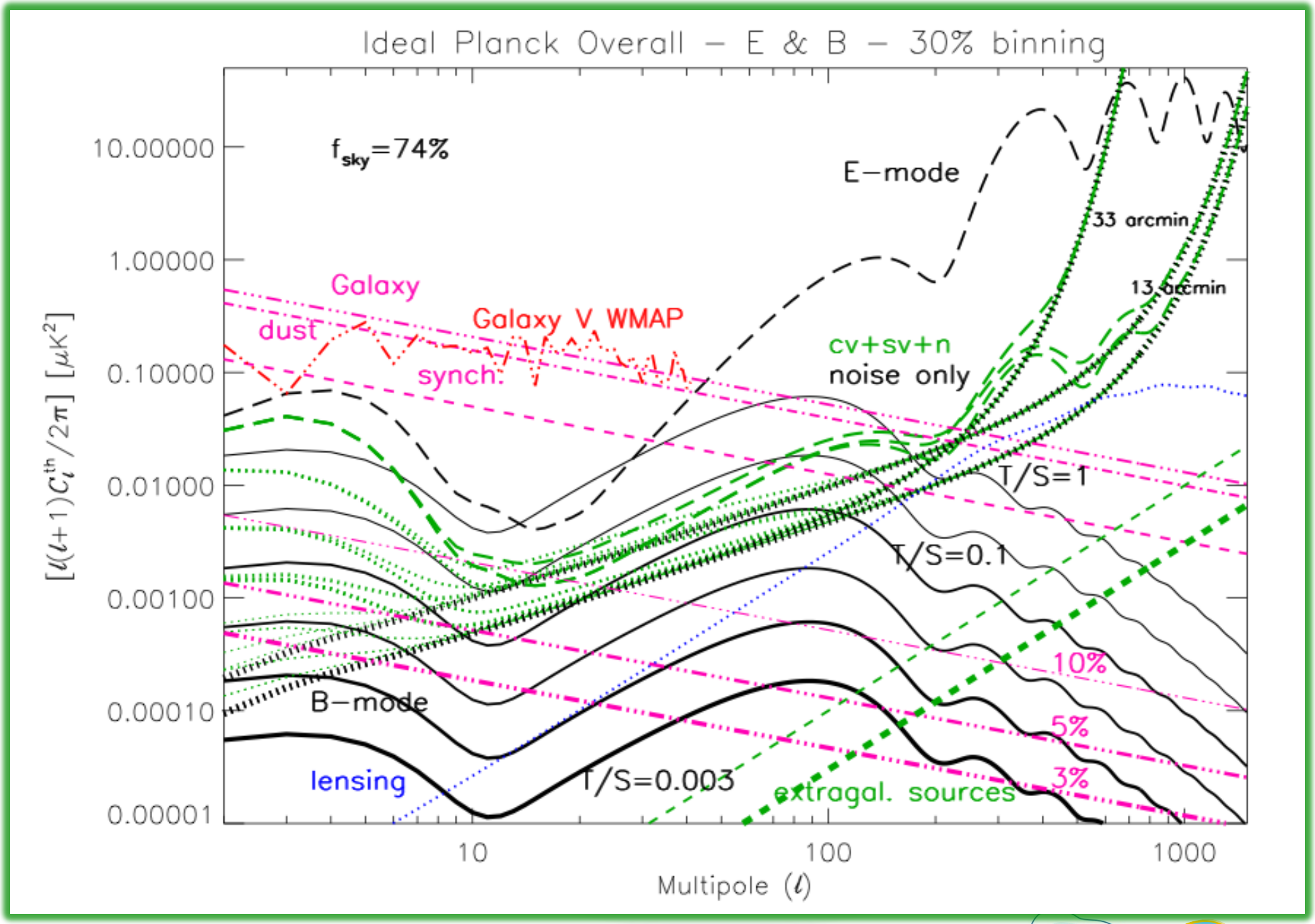
Ideal Planck Overall – E & B – 30% binning
f_{sky}=74%
E–mode
33 arcmin
13 arcmin
Galaxy
dust
Galaxy V WMAP
synch.
cv+sv+n
noise only
T/S=1
T/S=0.1
10%
5%
3%
B–mode
lensing
T/S=0.003
extragal. sources
10.00000
1.00000
0.10000
0.01000
0.00100
0.00010
0.00001
10
100
1000
Multipole (ℓ)
$[\ell(\ell+1)C_\ell^{th}/2\pi]$ $[\mu K^2]$

Future CMB missions:

COrE (or new M idea)
PRISM (L mission)

http://www.prism-mission.org/

Please,
sign to support !

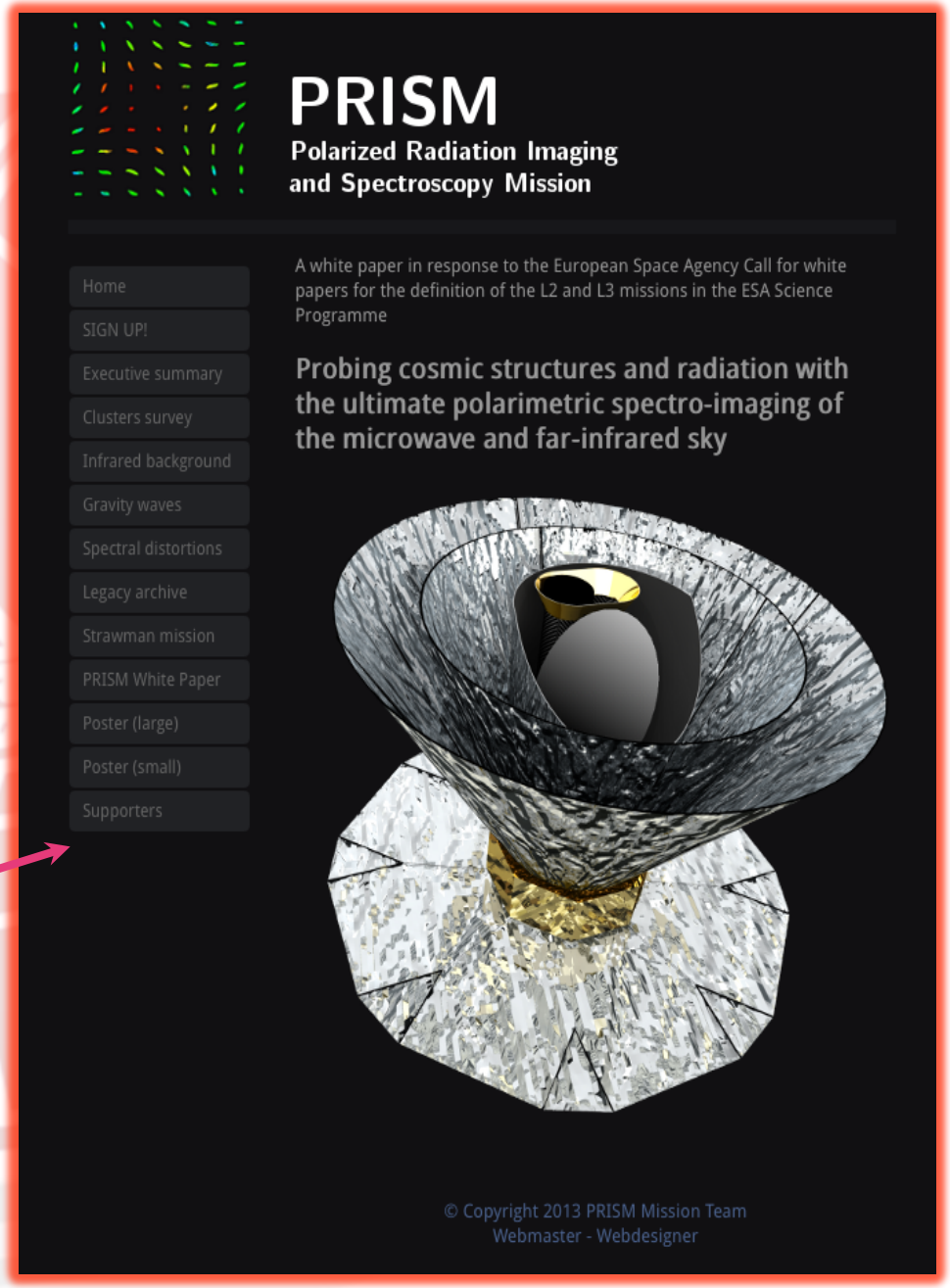

In a nutshell:

New science with a polarimetric and spectral survey of the **Hubble volume** from the μ–wave to the far-IR

Ultimate galaxy cluster survey via Sunyaev-Zeldovich effect (SZ): (>10^6 : all clusters with $M>10^{14}M_\odot$ within our horizon)

1

Legacy archive of hundreds of full-sky intensity and polarization maps from tens of GHz to few THz with extreme precision and resolution :
$1\mu K_{CMB}$arcmin
1'FWHM@λ1mm

6

Ultimate measurement of CMB polarization, Gaussianity, and absolute spectrum.
Search for the gravitational waves produced during inflation.

5

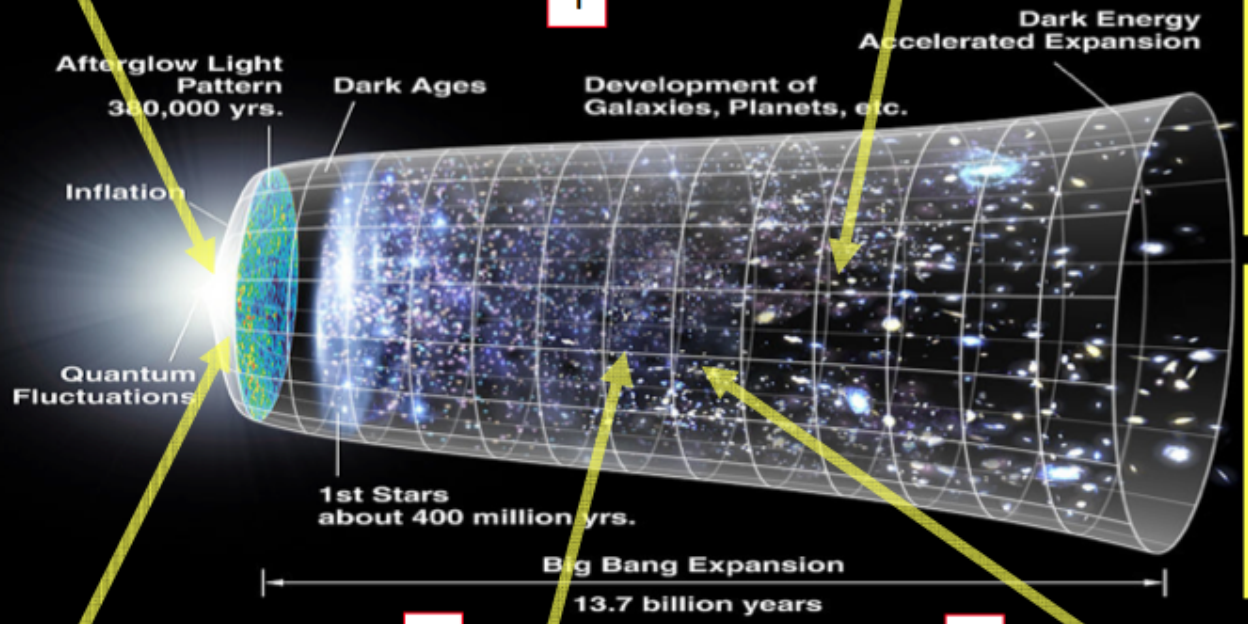

A complete survey of the interstellar medium in the Milky way : dust, molecular lines, magnetic field, ...

4

Probe epochs before recombination and new physics using CMB spectral distortion measurements

3

Map the gravitational potential all the way to z=1100 through CMB lensing

2

Probe early star formation and its evolution through precision characterization of the Cosmic Infrared Background (CIB)

Measuring B-modes

- Measuring B-modes to r=0.001 will require **exquisite control of polarized foregrounds**.
- Current extrapolations with the simplest allowed foreground models predict that the galactic foreground will outshine the r=0.001 primordial by about x100 in all frequency channels, and emission properties are likely to be more complicated than many of the optimistic foreground forecasts suggest
- While forthcoming experiments could find hints of cosmological B modes, **only a large mission with wide frequency coverage and high angular resolution can provide a reliable and convincing detection.**

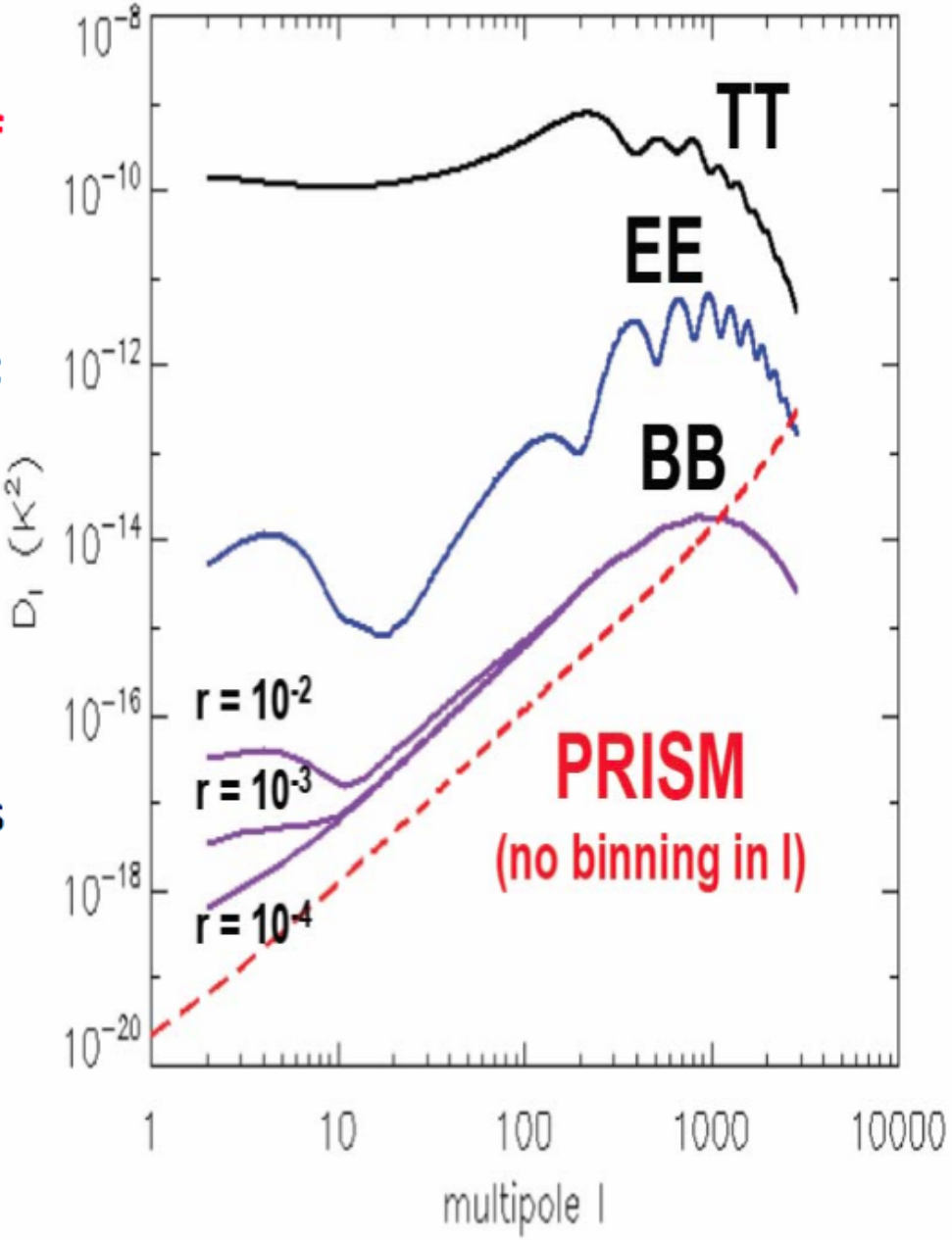

Reionization: radiative feedback

The increase of temperature in ionized region leads to a dramatic suppression of the formation of low-mass galaxies.

Suppression model (CF06): radiative feedback is effective in dark matter haloes with circular velocity below a critical value $v_{crit} \sim (2k_B T/\mu m_p)^{1/2}$ where T is the average temperature of ionizing regions [~ 30 km/s for $T=3\times10^4$ K]

Filtering model (G00): the average baryonic mass within haloes in photoionized regions is a fraction of the universal value:

$$\frac{M_b}{M} = \frac{\Omega_b / \Omega_m}{[1+(2^{1/3}-1)M_C / M]^3}$$

where M_C is the mass of haloes that retain 50% of their gas mass (Gnedin 2000)

Astrophysical reionization models

We implemented these two radiative feedback prescription in a well tested reionization model (Choudhury & Ferrara 2006).

The main features of the model are:

- **Inhomogeneous reionization** assuming lognormal overdensity distribution
- **Sources of reionization**:
  - PopIII stars: Salpeter IMF but metal free (Schaerer 06)
  - PopII stars: Salpeter IMF, Bruzual & Charlot
  - Quasars: important for z<6
- **Chemical feedback** governs the transition from PopIII to PopII stars ($Z_{crit}=10^{-5+/-1}\ Z_{sun}$): the two populations are coeval and PopIII stars can form also at relatively low-z.

Extension to all modes
B-modes & reionization beyond simple tau-approximation

- Future of CMB polarization anisotropies:
  - towards B-modes & full exploitation of all modes
- Implementation of reionization models in CAMB code considering all modes & in particular B-modes (T. Trombetti & C. Burigana, 2012, JMP, 3, 1918)
- Inclusion of
  - Phenomenological models (high/low z)
  - Astrophysical models
  - Mix of models

Typical cases →

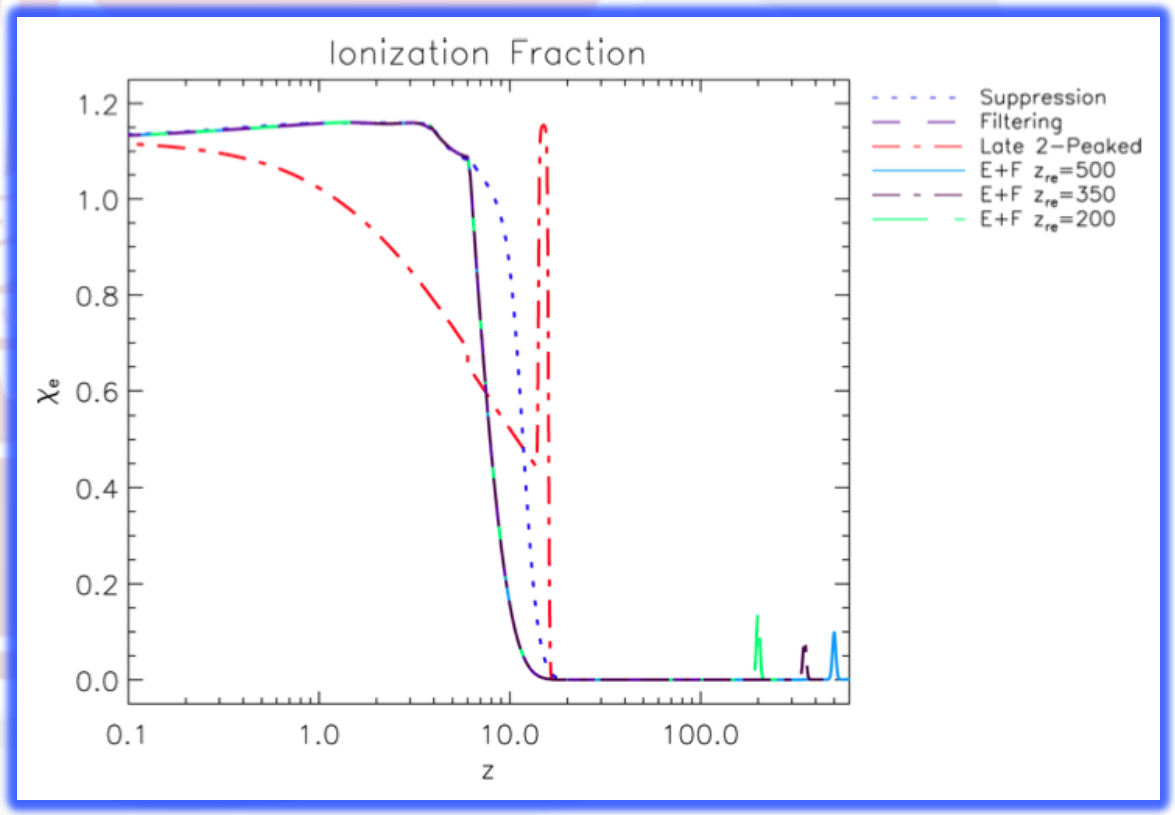

EE & BB predictions

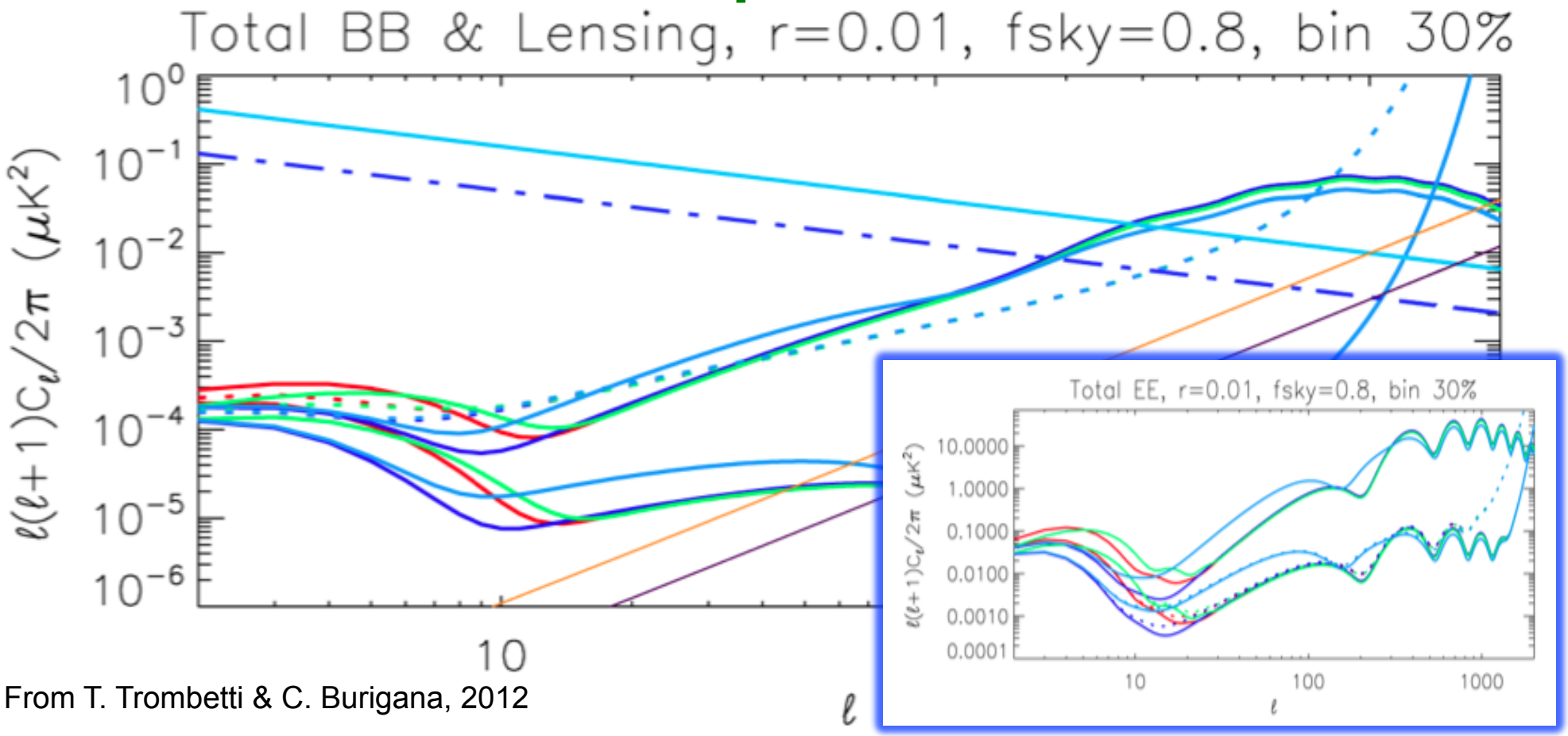

From T. Trombetti & C. Burigana, 2012

- Suppression, τ=0.1017
- Planck CV+N
- COrE CV+N
- Filtering, τ=0.0631
- Planck CV+N
- COrE CV+N
- Synchrotron, ν_{cmb}=70 GHz
- Radiosources

- Late Double Peaked, τ=0.1017
- Planck CV+N
- COrE CV+N
- Early & Filtering, τ=0.1017
- Planck CV+N
- COrE CV+N
- Dust, ν_{cmb}=70 GHz
- Radiosources 30%

Reionization BB: comparing models & experiments

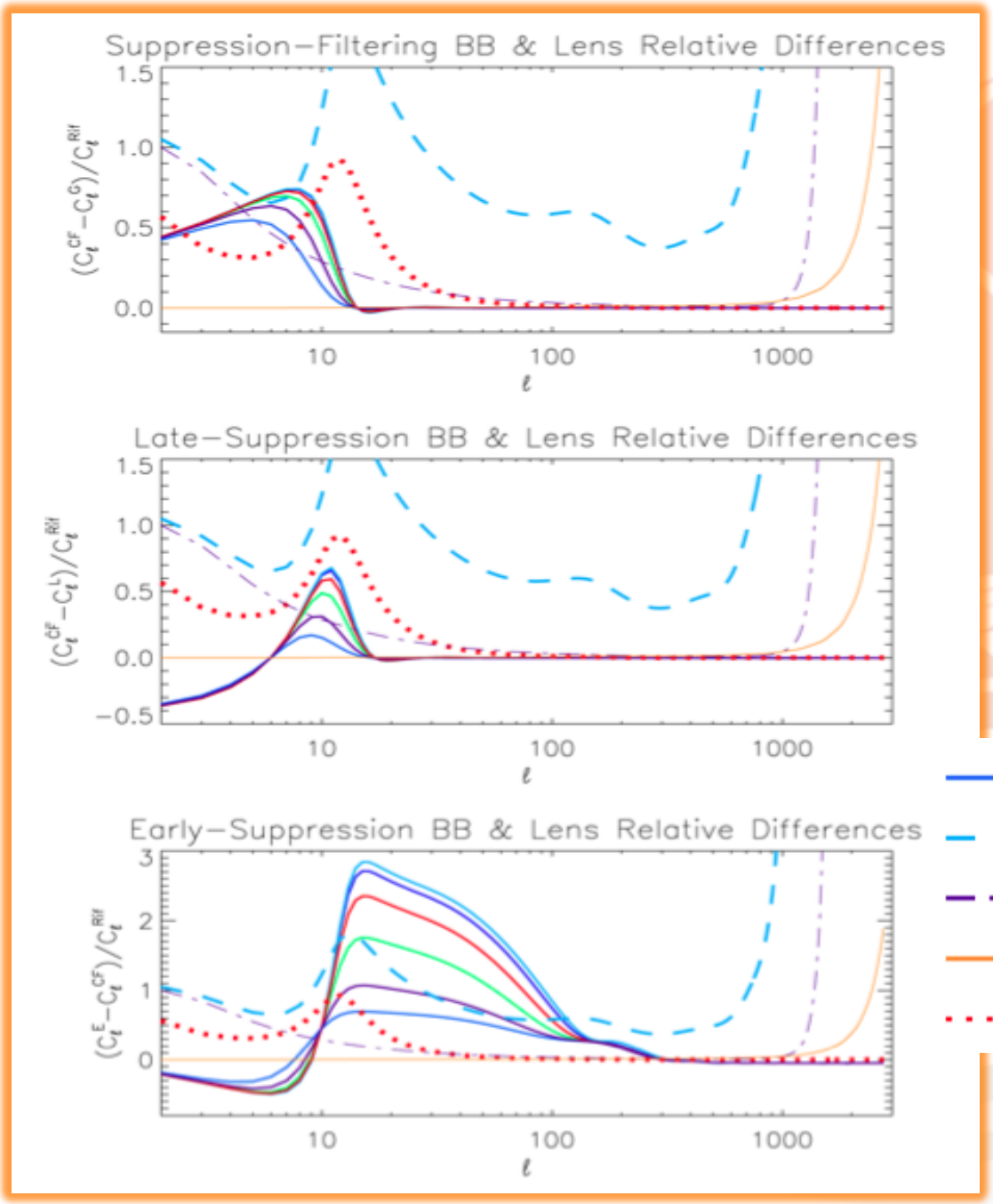

r=0.3
r=0.1
r=0.03
r=0.01
r=0.003

r=0.001
Planck N+CV r=0.03
COrE N+CV r=0.03
Radio 30% suppress
S+D 3%Map r=0.03

From T. Trombetti & C. Burigana, 2012

Temperatures: [kinetic, CMB spin (21 cm)]

Synergy with all-sky 21cm background signal

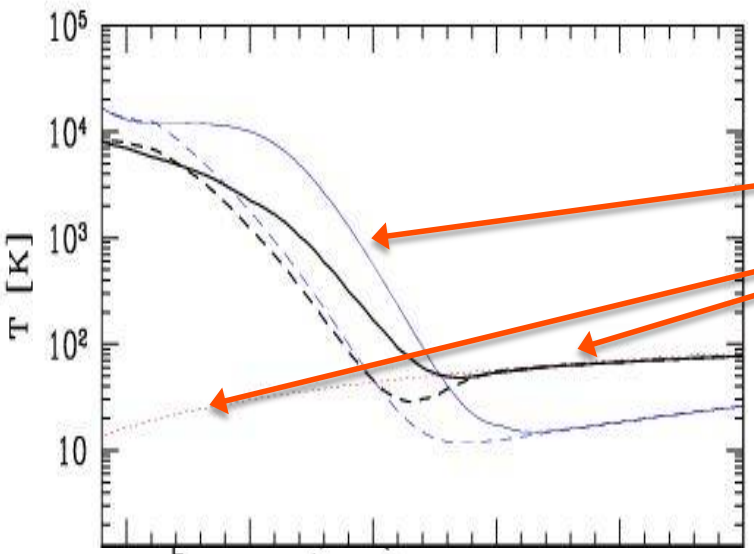

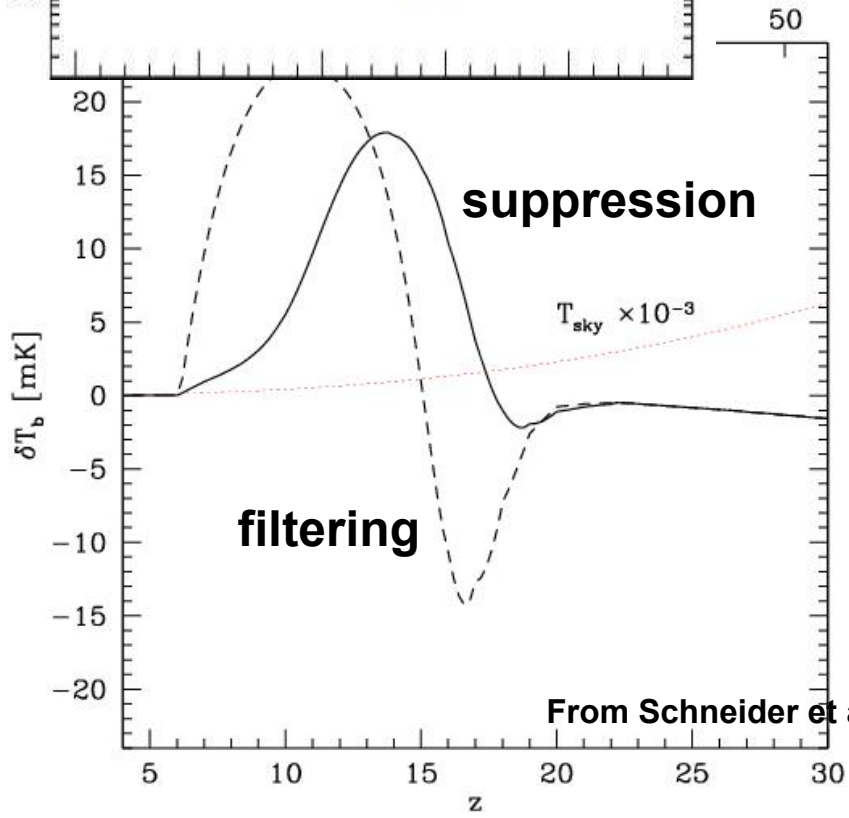

From Schneider et al. 2008, MNRAS, 384, 1525

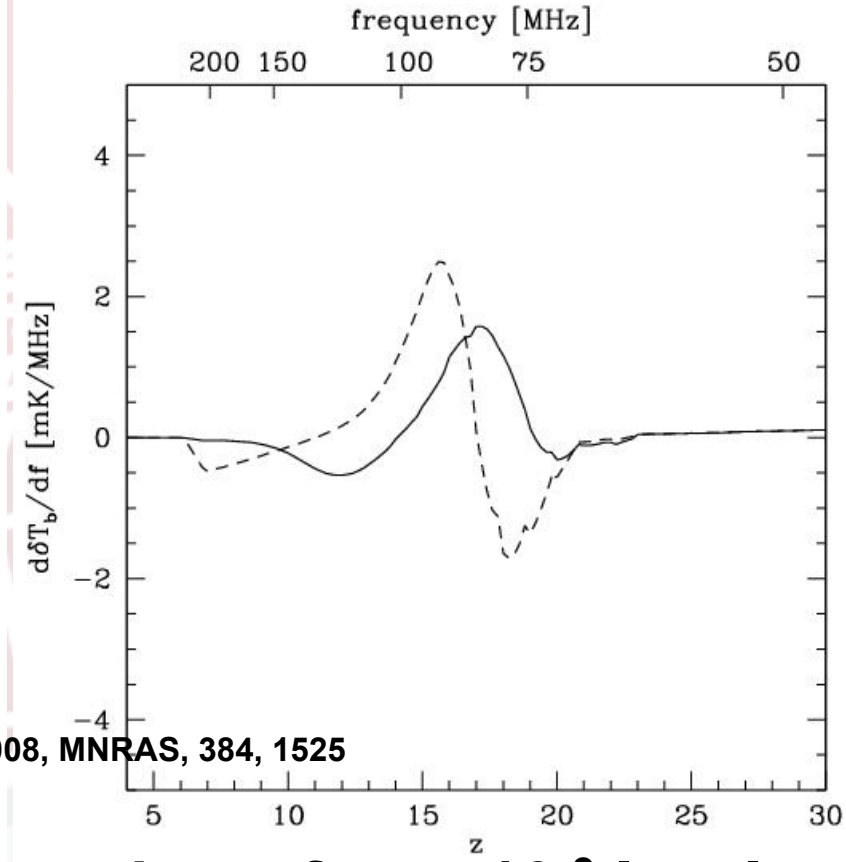

require removal of foreground at a few x 10^{-3} level

21cm signal: detectability filtering - suppression

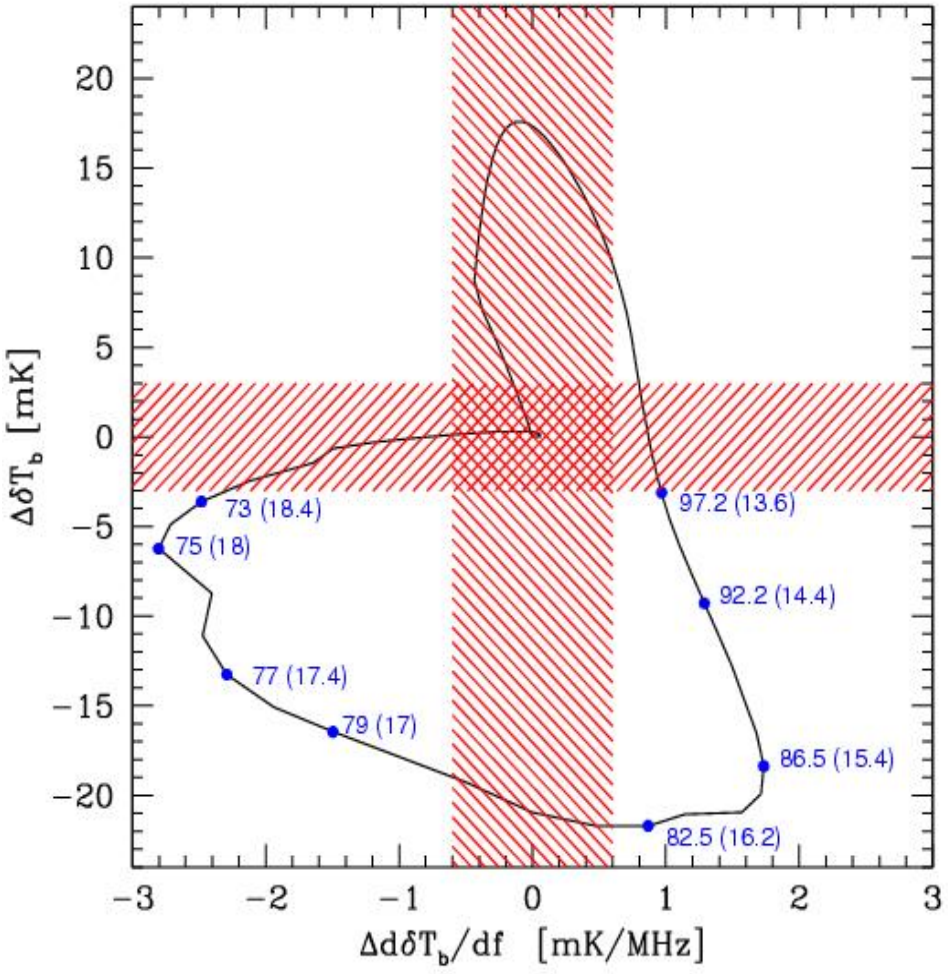

A successful detection requires:

$\Delta\delta T_b > 3$ mK

$\Delta(d\,\delta T_b/df) > 0.6$ mK MHz^{-1}

Single-dish, all sky 21cm observations can discriminate between the two model in the frequency ranges

ν_{obs} = 73-79 MHz (z=17-18.4)

ν_{obs} = 82.5-97.2 MHz (z=13.6-16.2)

From Schneider et al. 2008, MNRAS, 384, 1525

Probing the Universe with galaxy clusters

- The combination of extreme sensitivity, broad spectral coverage, and angular resolution of ***PRISM*** are used to separate the SZ component cleanly from other foregrounds, allowing the following new science:

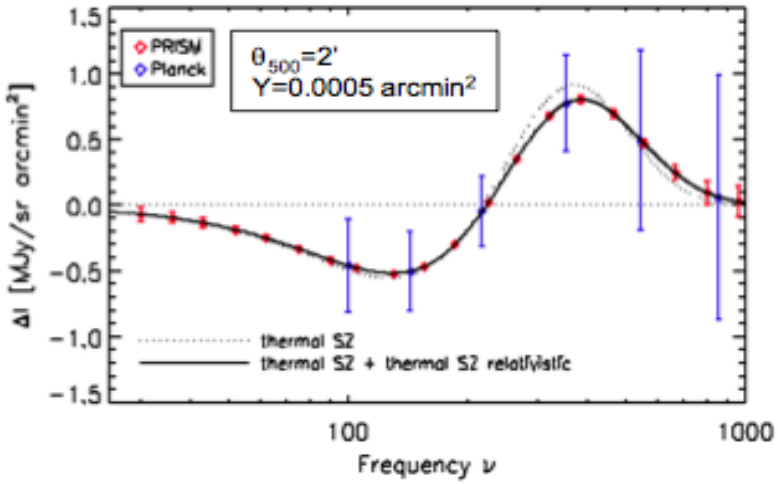

- detect cluster and groups systems **throughout the Hubble volume** from the moment just after their formation.
- Measure cluster mass to high redshift (z>4) through gravitational lensing of the CMB (temperature & polarization). **Detection limit below $10^{14}M_{\odot}$ at all redshifts.**
- Measure the kinetic SZ effect, with typical errors of 50 km/s for individual clusters. **This (and only this) will allow mapping the *cosmic velocity field*. A new probe of dark energy and large scale structure.**

Probing the Universe with galaxy clusters

- **Cluster catalog:** realistic simulations show that the PRISM cluster catalogue wil include >10^6 clusters, with mass limit <$10^{14} M_\odot$ at all z.
- **Cosmology probe:** This will allow to constrain cosmological parameters (mainly σ_8 and Ω_m, but also w_a and w_o).
- **Cosmic velocity field**: The peculiar velocity of a few ~10^5 galaxy clusters will be measured
- **Relativistic corrections and non-thermal effects**: the temperature of the hot gas will be measured for ~10^4 galaxy clusters

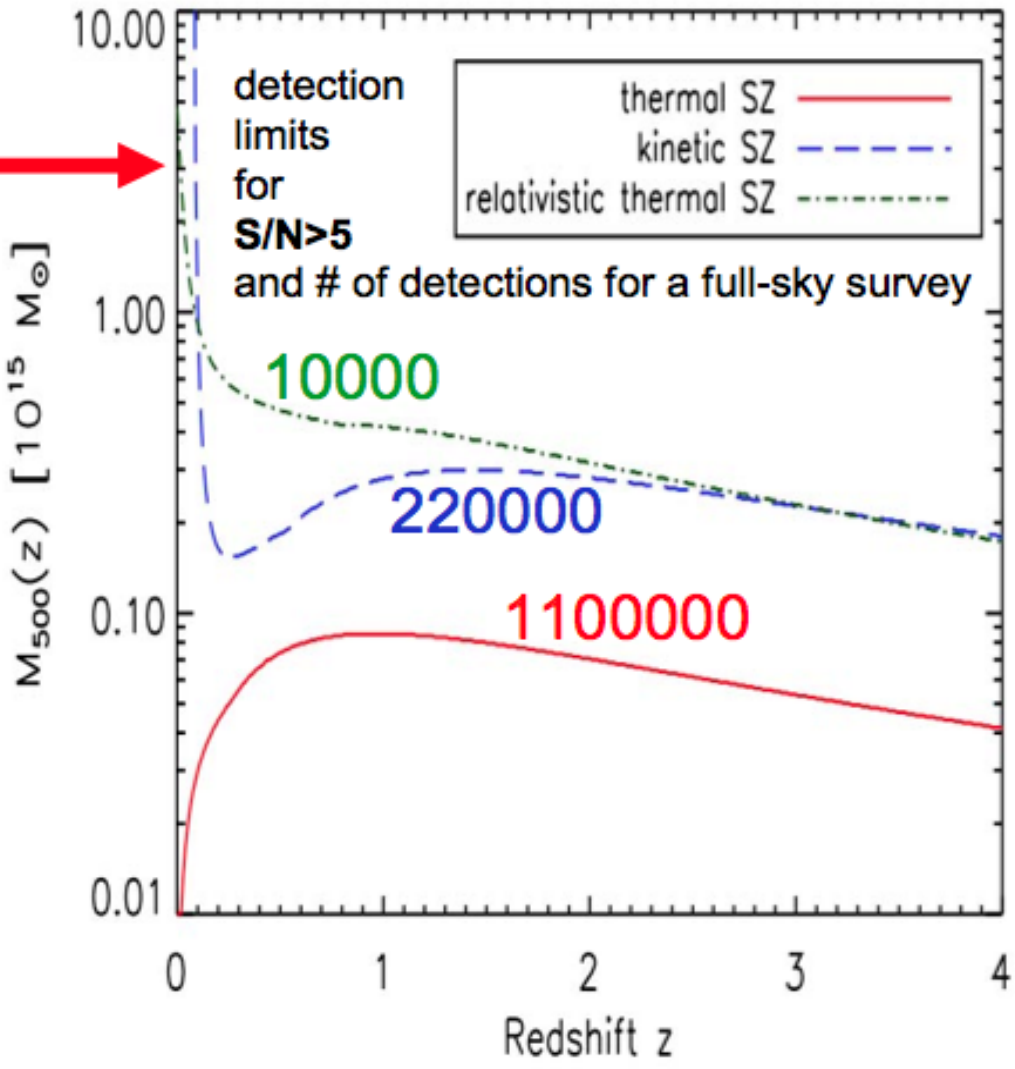

SZ effect with SKA towards galaxy clusters

- The identification of about one thousand of galaxy clusters with the XMM-Newton and Planck ESA satellites is on-going, while observations of many thousands of clusters (~ 5×10^5) come from the SDSS.
- The typical angular sizes of galaxy clusters range from ~ arcmin to few tens of arcmin.
- With the the SKA collecting area it will be possible to accurately map the SZ effect of each considered cluster, particularly at moderately high z, with a precise subtraction of discrete radio sources.
- The combination with X-ray images, in particular with those proposed to ESA for the Athena+ (formerly XEUS) satellite project, designed to reach ~ arcsec resolution on a few arcmin FOV, will allow to accurately map the thermal and density structure of the gas in galaxy clusters.
- Also, remarkable will be the synergy with the optical and infrared (IR) surveys at ~ arcsec resolution expected in about ten years from the ESA Euclid satellite.

Thermal SZ effect at galaxy scale

- The proto-galactic gas is expected to have a large thermal energy content, leading to a detectable SZ signal, both when the protogalaxy collapses with the gas shock-heated to the virial temperature (Rees & Ostriker '77, White & Rees '78 [3,4]), and in a later phase as the result of strong feedback from a flaring active nucleus (Ikeuchi '81, Platania et al. '02 [5-7]).
- The angular scales of these SZ signals from galaxies are of the order of ≈ 10″, then of particular interest for a detailed mapping with the SKA and Athena in the radio and X-ray, respectively.
- The probability of observing these SZ sources on a given sky field at a certain flux detection level and the corresponding fluctuations are mainly determined by the redshift dependent source number density per unit interval of the SZ (decrement) flux.
- The lifetime of the considered SZ sources is crucial to determine their number density.

Thermal SZ effect at galaxy scale

- In spite of the many uncertainties of these models, it is remarkable that the CMB fluctuations (dominated at small scales by the Poisson contribution) induced by the SZ effect of these source populations could contribute to the CMB anisotropy power at high multipoles (see the figure in next page for a comparison with CBI and BIMA data).
- In general, a direct probe of these models and, possibly, their accurate knowledge through a precise high resolution imaging is highly interesting. The figure in next page shows the number counts at 20 GHz predicted by these models: in a single SKA FOV about few × 10^2 – 10^3 SZ sources with fluxes above ~ 100 nJy could be then observed in few hours of integration.
- Given the typical source sizes, we expect a blend of sources in the SKA FOV at these sensitivity levels, while much shorter integration times, ~ sec, on many FOV would allow to obtain much larger maps with a significant smaller number of resolved SZ sources per FOV.
- Both surveys on relatively wide sky areas and deep exposures on limited numbers of FOV are interesting and easily obtainable with SKA.

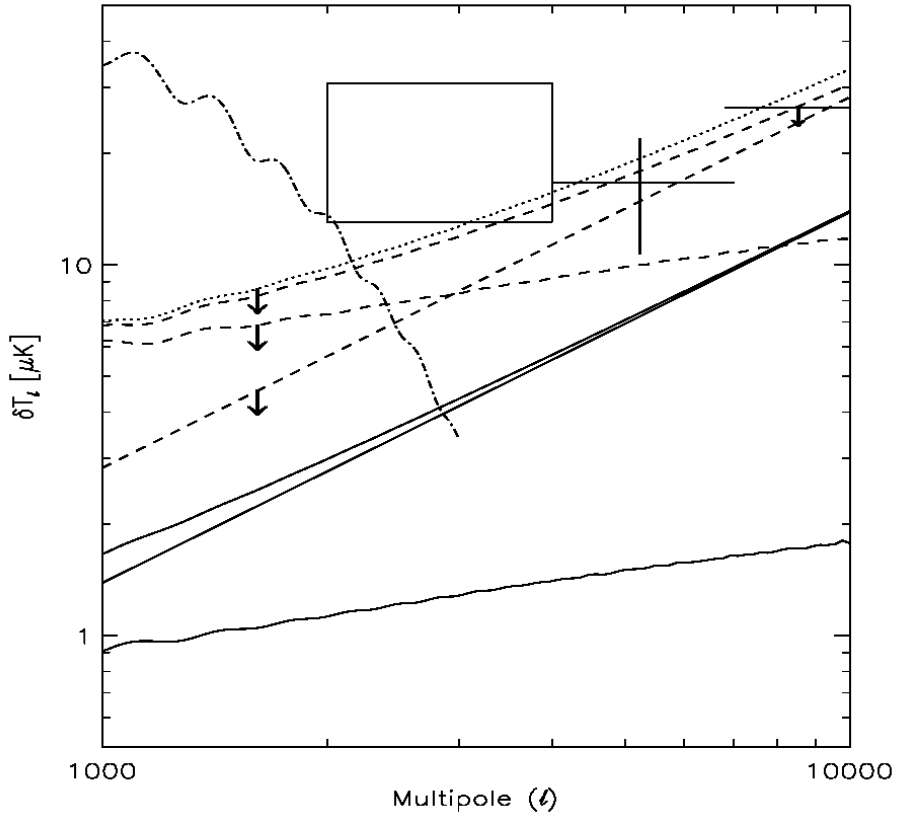

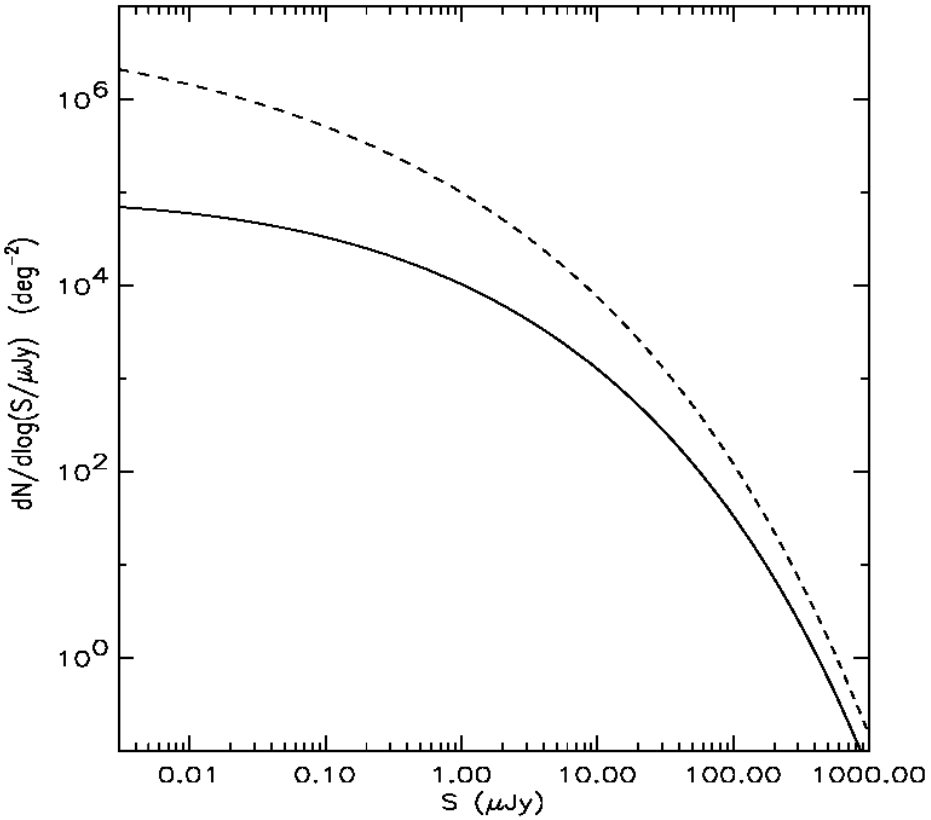

Angular power spectrum of SZ effects at 30 GHz compared to CMB primary fluctuation power spectrum and CBI (box) and BIMA (data points) measures. Solid lines represent clustering (bottom line), Poisson (middle line) and global (upper line) contributions from quasar driven blastwaves. Dashed lines represent clustering (bottom line at high ℓ), Poisson (middle line at high ℓ) and global (upper line) contributions from proto-galactic gas. The latter are actually upper limits since, because of the uncertainty in the cooling time, the extreme assumption that $t_{cool} = t_{exp}$ has been adopted in the computation. Dots refer to the overall contribution.
From Burigana et al. '04 [8].

Number count predictions at 20 GHz for SZ effects as function of the absolute value of the flux from proto-galactic gas heated at the virial temperature (dashes) assuming $M_{gas}/M_{vir} = 0.1$ and from quasar driven blast-waves (solid line). The exponential model for the evolving luminosity function of quasars is derived by Pei '95 [9] for an optical spectral index of quasars $\alpha = 0.5$ ($S_\nu \propto \nu^\alpha$). The parameters have been set at $\varepsilon_{BH} = 0.1$, $f_h = 0.1$, $k_{bol} = 10$, $t_{q,opt} = 10^7$ yr.
From Burigana et al. '04 [8].

Free-free signals: Ionized halos at high z

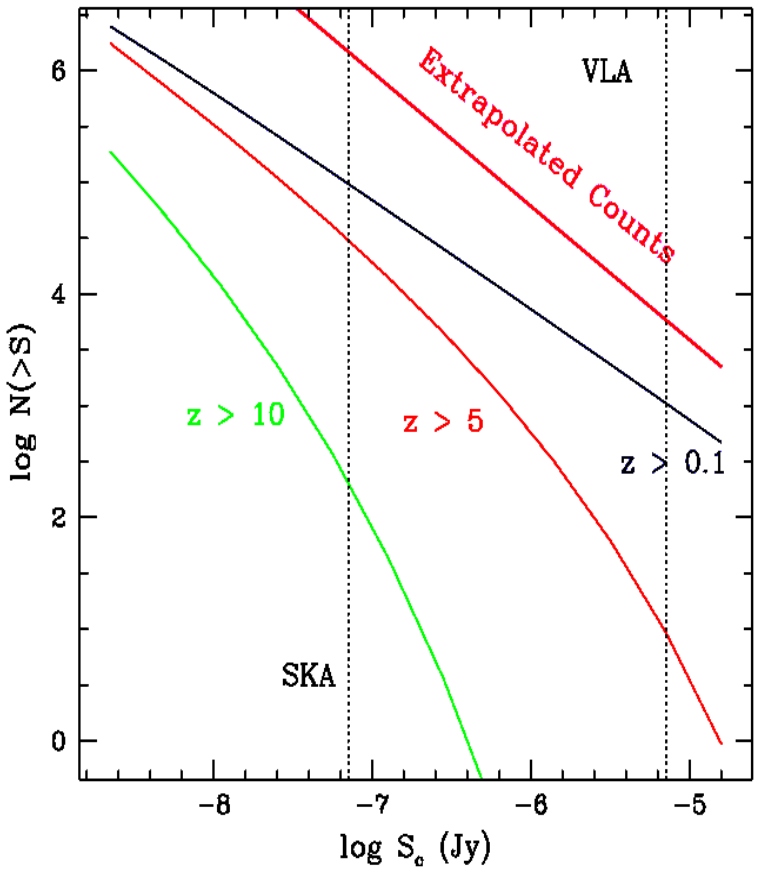

The understanding of the ionizing emissivity of collapsed objects and the degree of gas clumping is crucial for reionization models. The observation of diffuse gas and Population III objects in thermal bremsstrahlung has been investigated by Oh '99 [10]. A natural way to distinguish between free-free distortion by ionized halos is represented by high resolution observations of dedicated sky areas and by the fluctuations in the free-free background.

✧ In this model halos collapse and form a starburst lasting to = 10^7 yr, then recombine and no longer contribute to the free-free background.

✧ By adopting a Press-Schechter model, [] computed the number density of collapsed halos per mass interval and translated it in the cumulative number counts at different fluxes (see figure).

✧ SKA will allow to detect bright sources with deep exposures. SKA should be able to detect ~ 10^4 individual free-free emission sources with z > 5 in 1 □ above a source detection threshold of 70 nJy.

Number of sources which may be detected in the 1□ by SKA, as a function of the threshold flux S_c. Realistic limiting fluxes for point source detection are shown. The extrapolated source counts from Partridge et al. '97 [11] are also shown. From Oh '99 [10].

Free-free signals:
Individual halo at moderate z

Massive and dense clusters would produce a strong signal making the study of free-free emission in clusters at radio frequencies an interesting and useful way to study the intracluster medium.

✧ The figure shows a map of the free-free signal at 1 GHz extracted from a 300 Mpc simulation. The free-free distortion is of the order of 1 mK in the cluster regions.

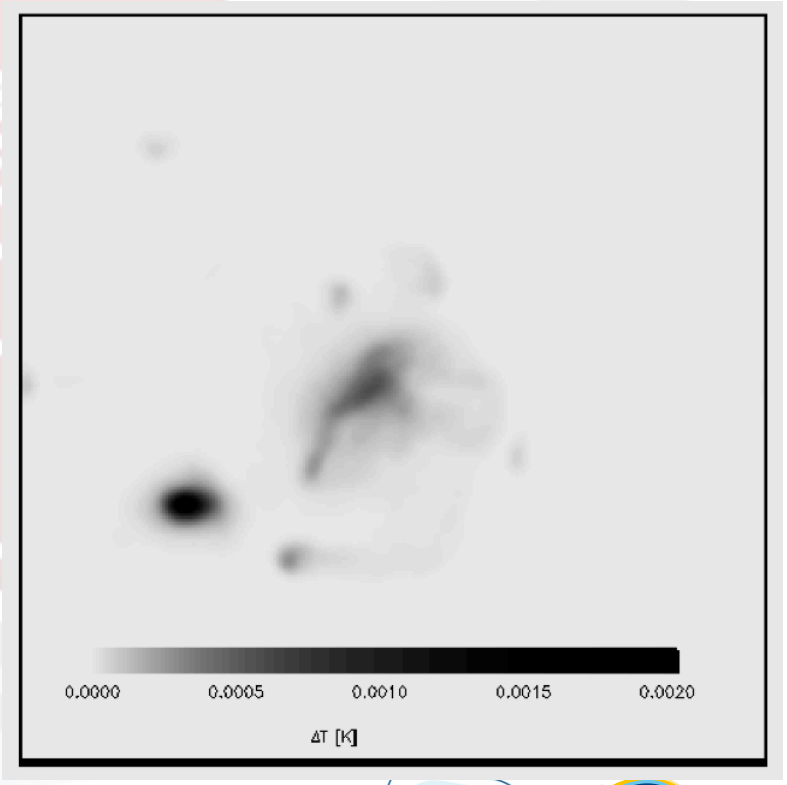

Free-free distortion for a massive halo,
$M = 6.6 \times 10^{14} h^{-1} M_{\odot}$, at redshift $z = 0.15$.
The greyscale shows the distortion in K and at 1 GHz.
The field of view is ≈ 40′.
The total flux in this region is
$S_{ff} = 2.83 \times 10^{-5}$ Jy.
From Ponente et al. ‘11 [12].

✧ SKA will be able to trace in detail the distribution of neutral hydrogen before reionization (through the 21-cm line) and the neutral-to-ionized Universe transition state at the reionization.

✧ Ponente et al. '11 [12] studied the regime of more massive halos focusing on the post reionization era, studying free-free radio emission from ionized gas in clusters and groups of galaxies with analytical models and simulations.

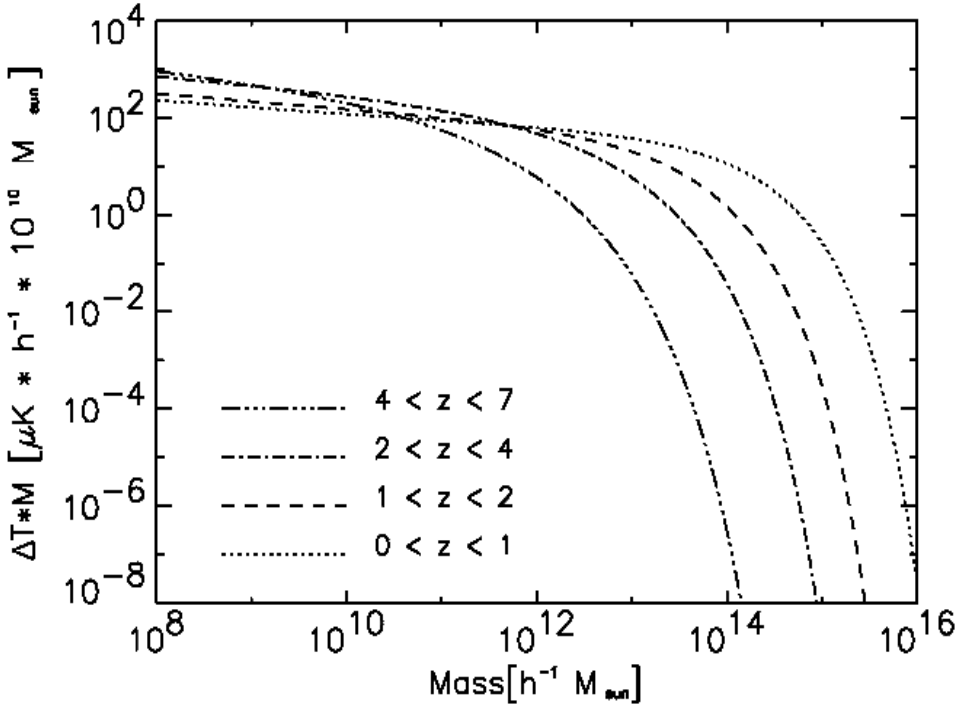

The figure shows the dependency of the average free-free distortion with the mass range for different redshift intervals. Smaller haloes contribute more to the average signal than massive ones at all redshifts. From Ponente et al. '11 [12].

✧ The cooling time is notably larger for massive haloes and highly non-linear phenomena like radiative cooling can be more easily ignored.

✧ **Combining a halo gas distribution model, as the β-model, with the haloes abundance as function of mass and redshift, it is possible to compute the mean free-free signal in a solid angle, function of redshift and/or mass.**

❖ Without any particular assumption about complex haloes physics, **a robust lower limit to the global averaged free-free distortion signal expected from the diffuse ionized IGM** in a given cosmological reionization scenario can be derived from fundamental arguments based only on density contrast evolution on cosmological models and well-known radiative emission mechanisms (Trombetti & Burigana '13 [13]:

- ✓ Boltzmann codes for the matter variance evaluation;
- ✓ a dedicated code for the free-free distortion including the correct time and frequency dependence of Gaunt factor.

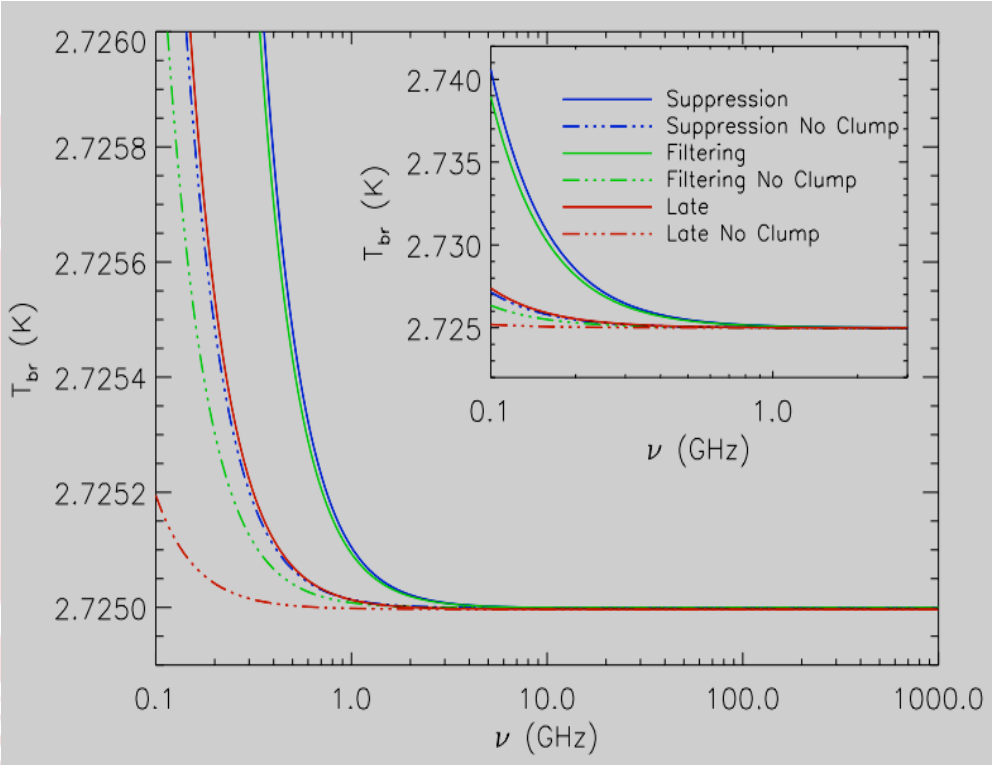

As shown in the figure, where signals from both free-free distortion and Comptonization decrement are included, the expected excess is at ~ mK level at decimeter wavelengths, a target clearly accessible to the SKA sensitivity.
To firmly detect this signal it is necessary to accurately observe the diffuse background level. A dedicated data analysis approach could be identified to this aim. From Feretti et al. '13 [14]

SKA contribution to future CMB spectrum experiments

- The current limits on CMB spectral distortions and energy dissipation processes in the plasma, $|\Delta\varepsilon/\varepsilon_i| \leq 10^{-4}$, are mainly set by the NASA COBE/FIRAS experiment.
- High accuracy CMB spectrum experiments from space, like DIMES at $\lambda \geq 1$ cm and FIRAS II at $\lambda \leq 1$ cm, have been proposed to constrain (or probably detect) energy exchanges 10–100 times smaller than the FIRAS upper limits possibly generated by heating (but also by cooling) mechanisms at different cosmic epochs.
- These perspectives have been recently renewed in the context of a new CMB space mission like PIXIE proposed to NASA or even in the possible inclusion of spectrum measures in the context of a polarization dedicated CMB space mission, of high sensitivity and up to arcmin resolution, like PRISM proposed to ESA.

To firmly observe such small distortions the Galactic and extragalactic foreground contribution should be accurately modelled and subtracted.

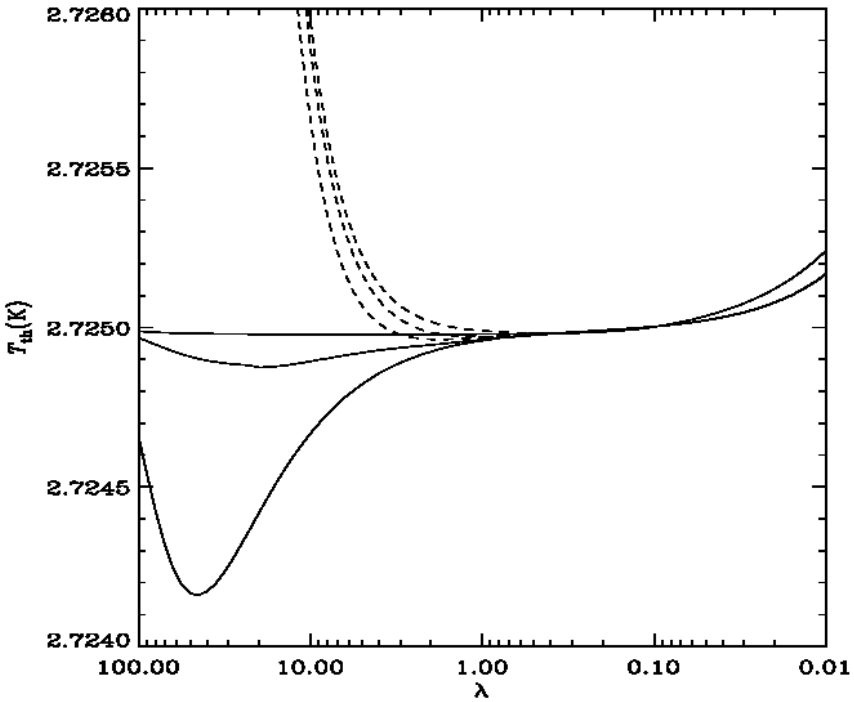

CMB distorted spectra as functions of the wavelength λ (in cm) in the presence of a late energy injection with $\Delta\varepsilon/\varepsilon_i \simeq 4y = 5 \times 10^{-6}$ plus an early/ intermediate energy injection with $\Delta\varepsilon/\varepsilon_i = 5 \times 10^{-6}$ occurring at the "time" Comptonization parameter $y_h = 5, 1, 0.01$ (from the bottom to the top; in the figure the cases at $y_h = 5$ – when the relaxation to a Bose-Einstein modified spectrum with a dimensionless chemical potential given, in the limit of small distortions, by $\mu \simeq 1.4\Delta\varepsilon/\varepsilon_i$ is achieved – and at $y_h = 1$ are extremely similar at short wavelengths; solid lines) and plus a free-free distortion with $y_B = 10^{-6}$ (dashes). From Burigana et al. '04 [8].

FF & other kinds of distortions in intensitiy

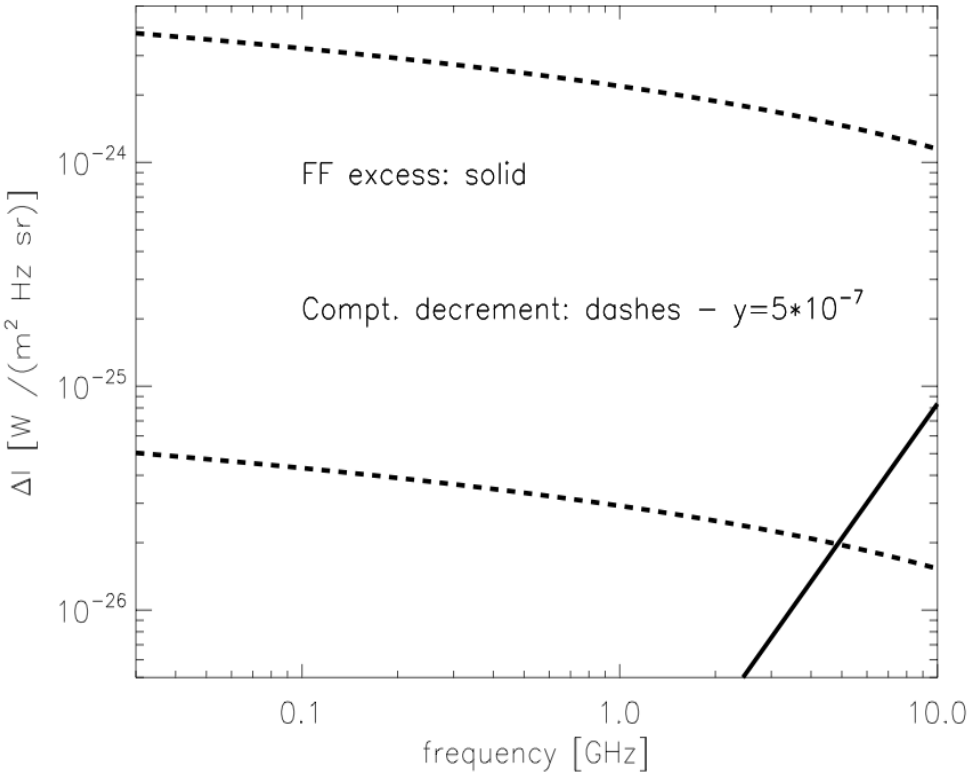

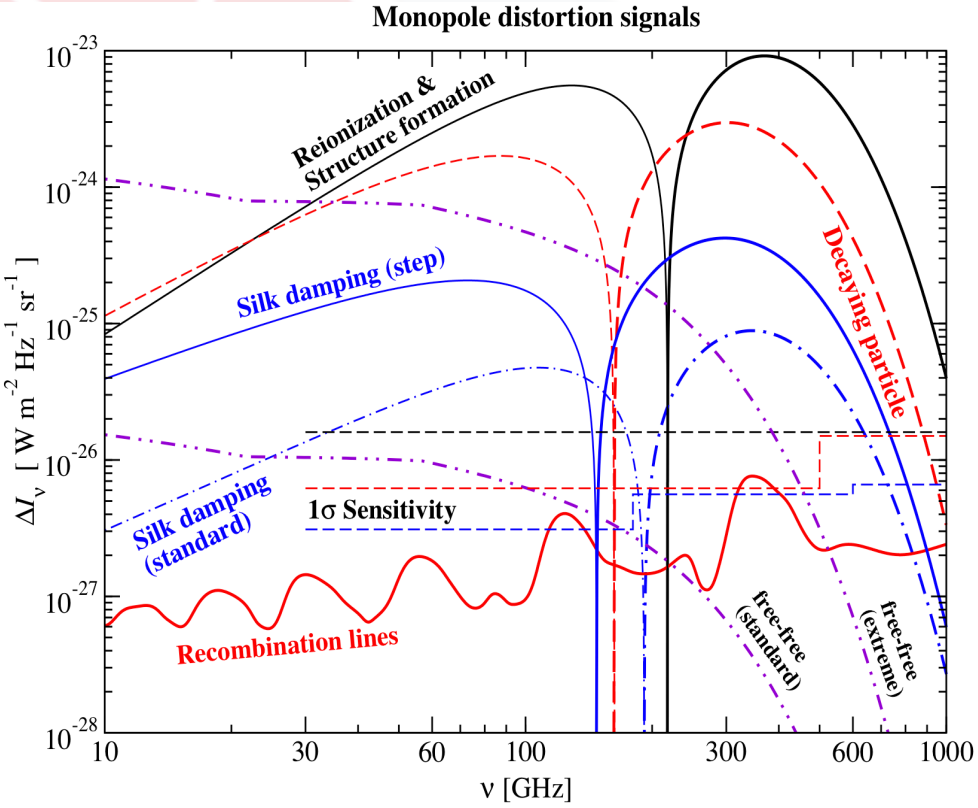

Low freqs. – SKA & ground experiments

High freqs. – Pixie, PRISM
From PRISM studies

- The very faint tail of radio source counts is essentially unexplored and their contribution to the radio background at very low brightness temperature is not accurately known.
- For illustration, with reasonable assumptions on differential source number counts, we find a contribution to the radio background at 5 GHz from sources between ~ 1 nJy and ~ 1 μJy between few tens of μK and few mK.
- These signals are clearly negligible compared to the accuracy of current CMB spectrum experiments, in particular at $\lambda > 1$ cm, but are significant at the accuracy level on CMB distortion parameters potentially achievable with future experiments.
- Differently from Galactic emission, it is isotropic at the angular scales of few degrees and can not be then subtracted from the CMB monopole temperature on the basis of its angular correlation properties.
- A direct radio background estimate from precise number counts will certainly improve the robustness of this kind of analyses.

- The relevance of this problem emerged in the detection by the NASA ARCADE 2 of an excess in the CMB absolute temperature at 3.3 GHz. Although this excess and its interpretations are controversial, this underlines how crucial is the precise estimation of very faint source counts for the exploitation of precise CMB spectrum measures.
- The SKA sensitivity at 20 GHz will allow the detection (to 5σ) of sources down to a flux level of ≃ 200 nJy (≃ 60,20,6 nJy) in 1 (10, 10^2, 10^3) hour(s) of integration over the ≃ 1 mas (FWHM) resolution element; similar numbers (from ≃ 250 to 8 nJy in an integration time from 1 to 10^3 hours, respectively) but on a resolution element about 10 times larger will be reached at ≈ GHz frequencies by using a frequency bandwidth of about 25%.
- Therefore, the SKA accurate determination of source number counts down to very faint fluxes can directly help the solution of one fundamental problem of the future generation of CMB spectrum space experiments at λ > 1 cm.

Cross-correlations between radio source catalogs & CMB maps

(see also Filipe Abdalla's talk)

✧ High CMB surveys, like those provided by *Planck*, typically cover a high sky fraction, f_{sky}, or even the whole sky. The SKA is mainly designed to achieve very faint fluxes on limited sky fields. On the other hand, the sensitivity of the SKA (SKA2_mid_dish in particular, but also SKA precursors) is so high on typical FoVs of ~ degree side at frequencies around one GHz, that it is reasonable to think to cover a significant sky fraction (thousands of square degrees) with unprecedented sensitivity accumulating some months of integration.

✧ A 1-yr SKA survey will contain > $10^9(f_{sky}/0.5)$ HI galaxies in at redshifts $0 < z < 1.5$.

✧ This makes the combination of *Planck* and SKA a powerful tool for improved cross-correlation analyses between CMB and radio data, that can be generalized to surveys in other frequency bands.

Cross-correlations between radio source catalogs & CMB maps

Cross-correlation & angular power spectrum

Given a CMB map in temperature and a galaxy survey x = (T, G) (vector in pixel space), the Quadratic Maximum Likelihood (QML) (Tegmark '97 [15]) provides an estimator of the angular power spectrum C_ℓ^X, with X being one of TT, TG, GG.

The QML estimator is well suited for such analysis for several reasons:

- ✓ it is optimal (i.e. unbiased and minimum variance);
- ✓ it is a computationally demanding method and can be currently applied only at modest resolution but this is not a problem for studying effects present at large angular scales for which where the computation is affordable on a supercomputer;
- ✓ it is pixel based, making trivial the masking process necessary because of foreground emission or incomplete sky coverage.

Applications to ISW effect

✧ The Integrated Sachs Wolf (ISW) effect results from the line of sight integral in the Sachs-Wolfe '67 equation [16]. It arises when CMB photons streaming across the Universe interact with the time evolving gravitational potential wells associated with the foreground large scale structure.

✧ The potential evolution leads to a net change of the photon energies as they pass through them. The ISW is a linear effect depending on the cosmological model, since it requires a change in equation of state of the cosmic fluid. The evolution/ variation of the gravitational potential is related to the linear density perturbations of matter. This change is important at early times, when the universe goes from being radiation dominated to matter dominated (early ISW), and at late times, as the dark energy (or curvature) takes over from the matter (late ISW).

✧ Unlike the early ISW, the late ISW is virtually uncorrelated with the CMB anisotropies generated at last scattering: the typical auto-correlation function for the ISW is shown in figure (from Crittenden et al '96 [17]) for a ΛCDM model.

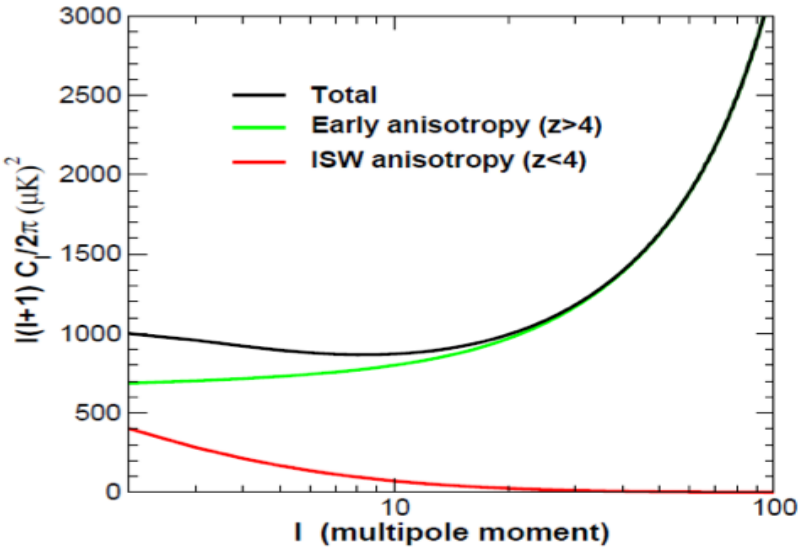

➢ **It is advantageous to isolate the late ISW generated at low redshifts through the cross-correlation of the CMB maps with LSS surveys:**

✓ CMB photons cross a time-varying potential and become slightly hotter or colder

✓ statistically, we expect a tiny correlation of hot spots in the CMB with LSS, an effect which expected to be less than 1 μK.

➢ **Interesting results have been already achieved from cross-correlating WMAP & SDSS and WMAP & NVSS (Raccanelli et al. '08, Schiavon et al. '12 [18,19]), opening the road for *Planck* & SKA analyses.**

Applications to non-Gaussianities

- Primordial perturbations at the origin of the LSS may leave their imprint in the form of small deviations from a Gaussian distribution. Different kinds of configurations, such as the so-called local type, equilateral, enfolded, orthogonal, have been predicted.
Their detection would have profound implications for inflationary mechanisms.

- Extragalactic radio sources are particularly interesting as tracers of the LSS, since they span large volumes up to high redshifts. Radio sources from NVSS, quasars from SDSS DR6 and DR7, LRG from SDSS II have been recently analyzed by Xia et al. '11 [20] also in combination with WMAP map:
  - f_{NL} = 48±20, 50±265, 183±95 at 68% CL for local, equilateral, enfolded configurations

- **Huge progress is expected combining *Planck* & SKA.**

Primordial magnetic fields (PMF)

✧ Large scale magnetic fields of the order of few μG observed in galaxies and galaxy clusters may be the product of the amplification, during structure formation, of primordial magnetic seeds (Ryu et al. '12 [21]).

✧ Models of early Universe predict the generation of PMF, either during inflation or during cosmological phase transitions (Widrow et al. '12 [22]).

✧ Constraints at the nG level come from CMB temperature power spectrum and bispectrum (Paoletti & Finelli '11, Caprini et al. '09 [23,24]).

✧ Gamma ray observatory *Fermi* have added new intriguing observations which might be interpreted as a lower bound for the amplitude of PMF.

✧ The data on gamma ray cascades from Blazars show a lack of photons which is compatible with diffuse extra-galactic magnetic fields in the intracluster medium (voids) with a lower bounds of the order of $10^{-15} - 10^{-16}$ G (Neronov & Vovk '10 [25]).

Primordial magnetic fields (PMF)

✧ If this lower bound for PMF will be confirmed, SKA can perform crucial measurements towards the probe of the generation mechanism.

✧ SKA measurement of very high-ℓ multipoles can improve these bounds on PMF as well as the characterization of foreground and secondary anisotropies beyond the Silk damping tail.

✧ The smoking gun of the Faraday rotation of CMB polarization anisotropies from intervening magnetic fields from a stochastic background of PMF is a B-polarization signal at very high-ℓ multipoles, $\ell \sim 10^4$.

✧ SKA observations can target such signal.

Galactic foregrounds versus Galactic astronomy

The accurate study of Galactic emissions is crucial for any cosmological exploitation of radio to infrared sky. In this context, Galactic emissions are considered as sources of foreground.

- As first probed by DASI, interferometers can be fruitfully used to map the diffuse sky signal on relatively wide areas in both total intensity and polarization, Fourier transforming data from the U-V space to the real 2D space.
- The possibility of extending this opportunity to intermediate and large scales, or equivalently to low and intermediate multipoles, largely relies on the capability of available mosaic techniques to assemble different FoVs into maps with appropriate large scale calibration and matching. This is of increasing complexity at SKA increasing frequency, since the smaller FoV sizes of higher frequencies.
- On the other hand, the high Galactic radio signal does not require the extreme accuracy demanded, for instance, by CMB fluctuation mapping at the SKA highest frequencies.

Galactic foregrounds versus Galactic astronomy

❖ **The SKA radio frequency coverage is of extreme interest to study the Galactic synchrotron emission, in both total intensity and polarization, and the unpolarized Galactic free-free emission.**

❖ **Extending the SKA frequency coverage to highest frequencies will allow to accurately derive the spectral behaviour of these emissions on a wide range. This is crucial for the accuracy of many component separation methods. In fact:**

- ✓ they take great benefit by the increasing of the frequency range of the templates adopted in the analysis and/or by a priori information about the spectral behaviour of the different components, related to the energy and properties of emitting particles, superimposed in the overall signal
- ✓ this information contributes to the improvement of the physical knowledge of the so-called mixing-matrix adopted in the inversion process that derives the different physical components from multifrequency maps.

❖ **Furthermore, SKA data can be used to map the Galactic HI 21-cm emission.**

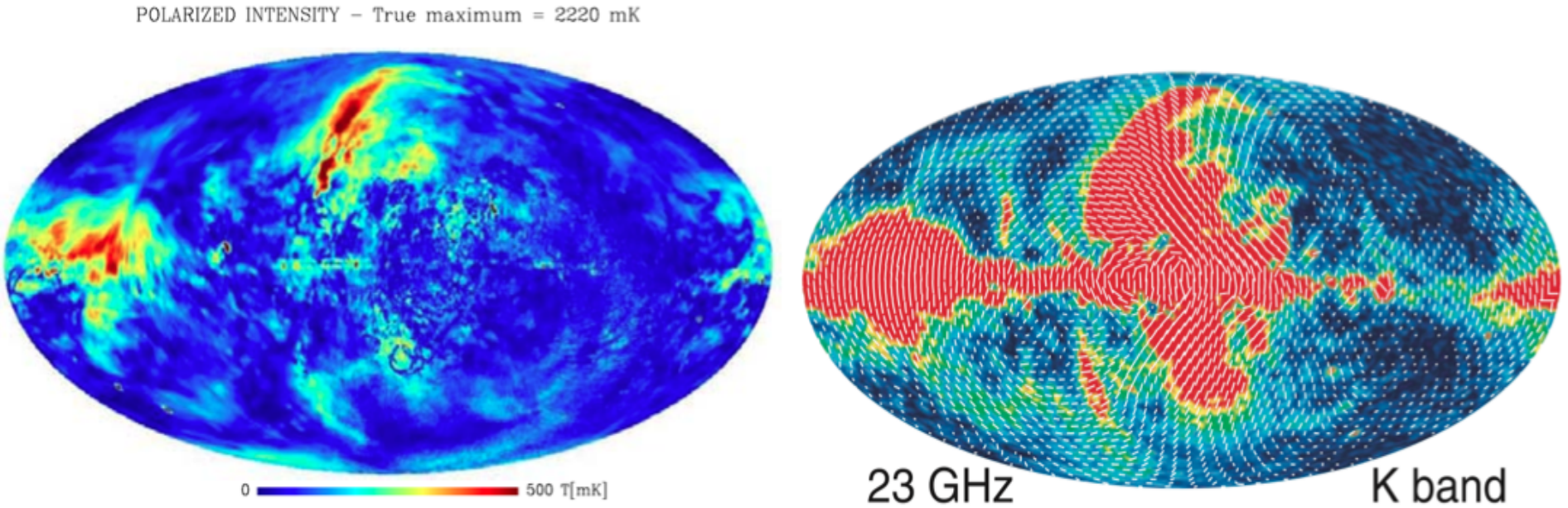

All-sky maps of Galactic polarized emission at radio (1.4 GHz, left image; from Burigana et al. '06 [26]) and microwave (23 GHz, right image; from Bennett et al. '13 [27]) frequencies.

Regarding the synchrotron emission, produced by relativistic cosmic ray electrons spiralling in the Galactic magnetic field, a remarkable feature of the Galactic radio sky is the significant depolarization appearing in a wide region around the Galactic center.
This effect is certainly much less relevant in the microwaves, as evident by the comparison of available radio surveys with millimeter surveys.

- If mosaic techniques will work successfully, a view of a very wide sky fraction will allow to map Galactic foregrounds at intermediate and large scales. This will have a tremendous impact for 3D physical models of the Galaxy and for the study of the large scale, almost regular component of the Galactic magnetic field.
- Turbulence phenomena predict a typical power law dependence of the power spectrum of diffuse emission with properties related to the physical conditions of the ISM in the considered area.
- Almost independently of the accuracy of mosaic techniques, SKA maps on many patches of sky of limited area will allow to reconstruct with unprecedented accuracy the correlation properties of the radio sky diffuse emission, thus providing crucial information for the comparison with theoretical models and and their implementation through numerical codes.

Multifrequency, high sensitivity radio observations with the SKA will certainly put a firm light on this problem, allowing to disentangle between the various depolarization effects:

- Faraday depolarization associated to Galactic magnetic fields
- geometrical depolarization coming from the averaging in the observed signal of contributions from cells with different polarization angles:
  - ✓along the line of sight
  - ✓within the angular directions of the observational effective beam.

Two other topics crucial for both Galactic science and foreground treatment for cosmology are the understanding of:

✓anomalous microwave emission

✓haze component

SKA will map the low frequency tail of these emissions.

Conclusions

- *Planck* worked & is working as expected
- Production of the most accurate CMB all-sky temperature anisotropy maps in the range 30-857 GHz ☺ … working on polarization for next year release in 2014 ☺
- Cosmological interpretation robust … but raises questions, e.g.
  - ✓ Neutrinos species/thermodynamics: N_{eff} compatible with "standard 3.046", but between 3 and 4 ???
  - ✓ Anomalies at large scales ???
- A next, ultimate CMB mission is crucial … & desired !
  - ✓ CMB polarization & distortions, recombination lines, clusters, far-IR galaxies/CIB, lensing, Galactic science, etc.
- Forthcoming/future radio facilities are promising!
- LOFAR, SKA & its precursors will answer to fundamental questions … & likely will raise new questions
- Complementarity/synergy between projects/analyses will be fundamental … & the future will be bright !